ALTISSIMO CONSULTING

# ROAD SURFACE NOISE

## Analysis of Low-Noise Asphaltic Mix Surfaces: Texture, Construction, and Porosity Effects

**Client:** Waka Kotahi / NZ Transport Agency
**Date:** May 2023
**Ref:** 22-105-R03-D

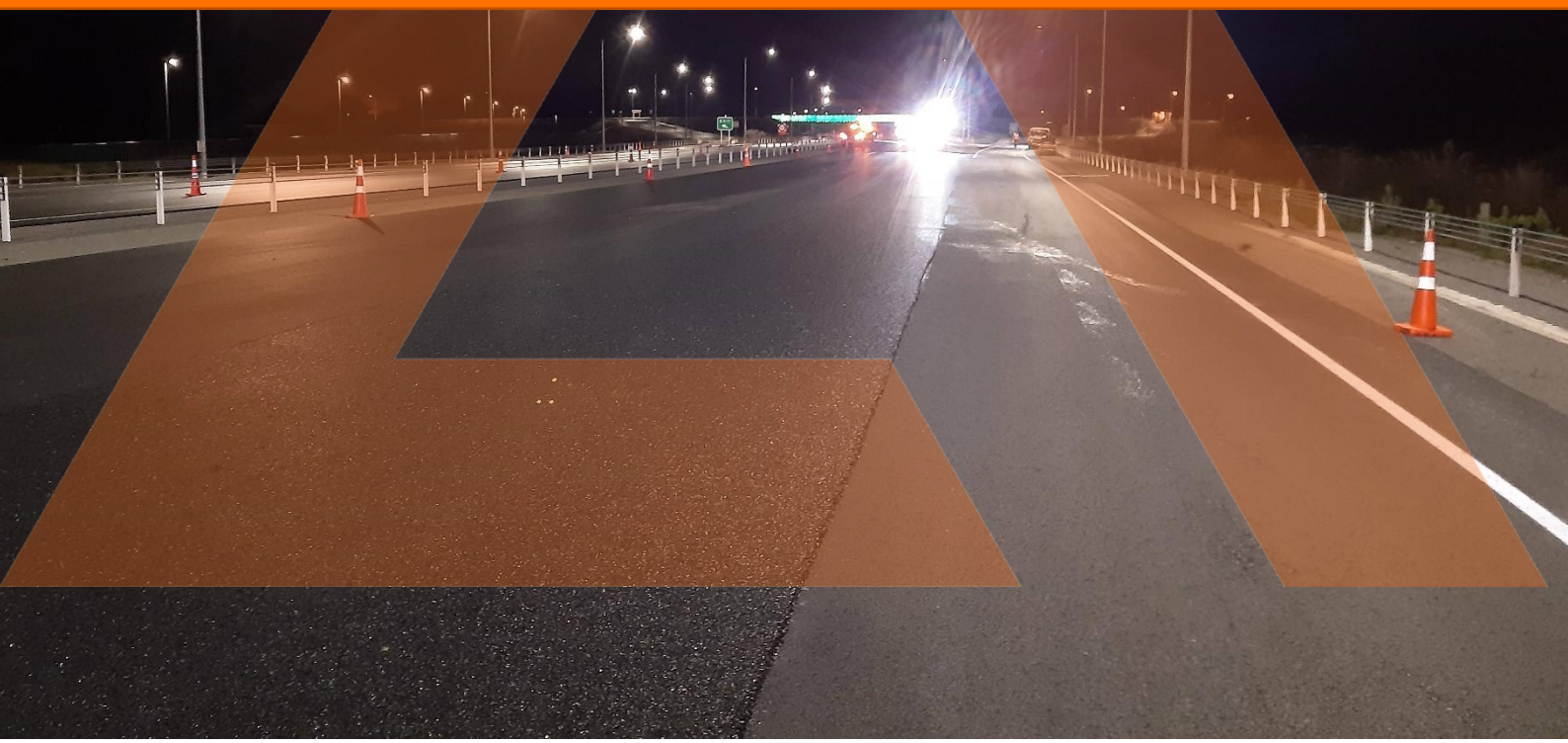

Prepared for (the Client)
**Waka Kotahi / NZ Transport Agency**

Prepared by (the Consultant)
**Altissimo Consulting Ltd**

| | |
|---|---|
| **Project** | Road Surface Noise |
| **Report** | Analysis of Low-Noise Asphaltic Mix Surfaces: Texture, Construction, and Porosity Effects |
| **Reference** | 22-105-R03-D |

**Prepared by:**

George Bell
Consultant

**Reviewed by:**

Robin Wareing
Principal Acoustics Engineer

Version history:

| Version | Date | Comment |
|---|---|---|
| A | 5/5/2023 | Preliminary report for client review |
| B | 21/5/2023 | Updated following client feedback. |
| C | 8/6/2023 | Updated construction method details. |
| D | 9/08/2023 | Clarified purpose of construction analysis. |

Report disclaimer and limitations:

This report has been prepared in accordance with the usual care and thoroughness of the consulting profession for the use of the Client. It is based on generally accepted practices and standards at the time it was prepared. No other warranty, expressed or implied, is made as to the professional advice included in this report.

This report should be read in full. No responsibility is accepted for use of any part of this report in any other context or for any other purpose or by third parties. This report does not purport to give legal advice. Legal advice can only be given by qualified legal practitioners.

# Abstract

This study is a continuation of Waka Kotahi's research of low-noise asphaltic surfaces. Three areas were explored: (1) the influence of macro-texture on noise, (2) the influence of construction parameters on surface properties, and (3) methods for measuring properties of porosity.

For the texture analysis, a tyre envelopment model was applied to high-resolution texture profiles captured using the stationary laser profilometer for four asphaltic surfaces. The indent depth, total drainage area, and RMS of the enveloped profile were identified as metrics having significant correlations with noise. Analysis of the spectral content of the enveloped profile provided insight into the excitation frequency and amplitude. The spectral analysis and metrics offered insight into the relatively low noise levels of the low void and high strength porous asphalt surfaces on the Christchurch Northern Corridor. The mean profile depth had strong correlations with all metrics, which supports its ongoing use for noise-related research.

The construction investigation was an observational study that explored the influence of paving and rolling parameters on texture, thickness, and noise. The results indicated that texture was negatively correlated with paving temperature, roller speed, and roller passes, but positively correlated with the time between paving and rolling. Thickness was negatively correlated with paver speed and positively correlated with the time between paving and rolling. Correlations between noise and construction parameters were complex and frequency-dependent, with inconsistencies in the correlations that could not be explained with the existing data. These results must be considered as indicative due to the low number of observations. It is recommended that additional surface properties are measured, and the correlation analysis is repeated to further investigate the influence of construction parameters on tyre/road noise.

Porosity influences noise through acoustic absorption and air flow dispersion into the surface. Methods of measuring acoustic absorption, air flow permeability, void content, and thickness were reviewed. It is recommended that the following measurements are considered: acoustic absorption following ISO 13472-1 (extended surface method), air flow permeability using a custom test apparatus, void content using a nuclear densometer, and thickness using a ground-coupled ground penetrating radar. The measurement data can then be used to expand the construction analysis.

# Contents

# Glossary

| | |
|---|---|
| CNC | Christchurch Northern Corridor |
| CPX | Close proximity |
| CSM2 | Christchurch Southern Motorway stage 2 |
| EPA | Epoxy-modified porous asphalt |
| Lane 1 | Closest lane to the centre of the road (see Figure 30). |
| Lane 2 | Second-closest lane to the centre of the road (see Figure 30). |
| $L_{CPX}$ | Close proximity sound pressure level. All measurements were conducted using the P1 tyre at a nominal speed of 80 km/h ($L_{CPX} = L_{CPX:P1,80}$) |
| MIT | Magnetic imaging tomography. Method used for measuring asphalt thickness. |
| MPD | Mean profile depth |
| $MPD_{HE}$ | MPD measured using the Road Science Hawkeye system |
| $MPD_{SLP}$ | MPD measured using the CAPTIF SLP |
| MTV | Material transfer vehicle |
| NB | Northbound |
| NDM | Nuclear densometer |
| p | Pressure |
| PA | Porous asphalt |
| PA7 HS | Porous asphalt high strength |
| PA7 LV | Porous asphalt low voids |
| Q | Air flow rate |
| RMS | Root mean square |
| SB | Southbound |
| SLP | Stationary laser profilometer |
| SMA | Stone mastic asphalt |
| TDA | Texture drainage area |
| WBB | Western Belfast Bypass |

# Background and Introduction

This investigation is a continuation on a previous study commissioned by Waka Kotahi (Bell, 2023). The study identified that variations in macro-texture and thickness of porous asphalt surfaces explain over 70% of the longitudinal variability in $L_{CPX}$ (for CSM2 and CNC). The cause of the variations in texture and thickness, and the residual 20-30% are not presently known.

A simplified hierarchy of the surface properties that influence tyre/road noise is shown in Figure 1. There are many more factors that have been omitted from the figure, but those present are hypothesised to be the dominant factors that can be influenced through design specifications and construction. A comprehensive review of parameters that affect tyre/road noise can be found in (Li, 2018).

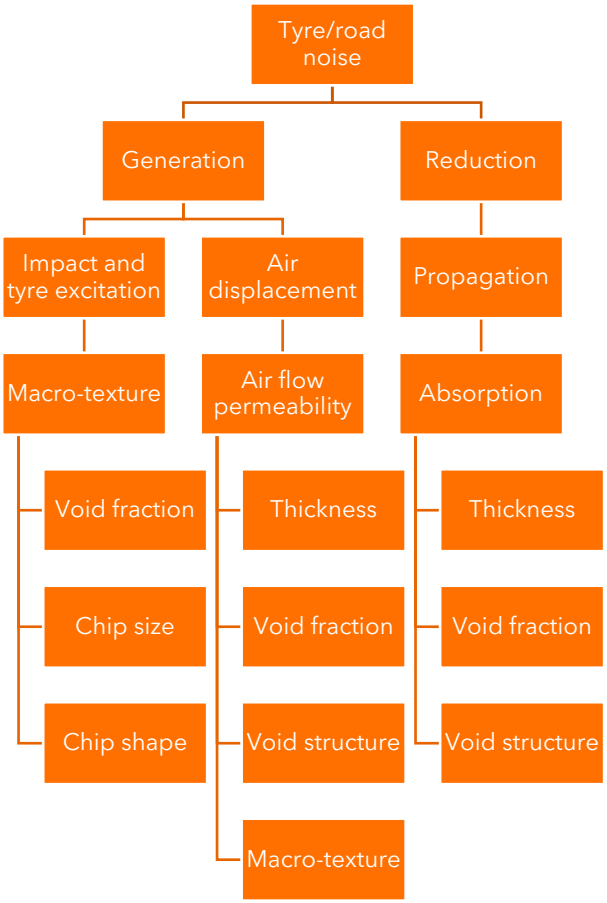


**Figure 1: Hierarchy of parameters influencing tyre/road noise.**

Surface characteristics that influence $L_{CPX}$ include texture, acoustic absorption (hereafter absorption), and air flow permeability. There are multiple other factors that affect noise, such as tyre properties, but these are out of scope for the current investigation.

The macro-texture (hereafter texture) of a road refers to the larger-scale features and irregularities on the surface, with longitudinal wavelengths between 0.5 and 50 mm. Texture induces forces on the rolling tyre, which result in excitation of the side wall and other noise generating mechanisms (Fong, 1998). Absorption affects noise through at least two mechanisms (Sandberg & Ejsmont, 2002): (1) reduces the "horn" effect in the leading and trailing edges of the tyre, and (2) attenuates noise as it propagates from the tyre. The air flow permeability allows for the dispersion of air into the road surface, reducing turbulent air flow noise (Winroth, Hoever, Kropp, & Beckenbauer, 2013).

Of the three direct surface characteristics that affect noise in this simplified model, only texture has been directly measured for the CNC project. Of the secondary properties, thickness was measured

periodically along the length of the road. Void content was measured during construction; however, the locations of the measurements are not known with sufficient accuracy to be correlated with $L_{CPX}$. This investigation aimed to undertake the following:

- Part I
  Use high-resolution profiles to understand how texture of asphalt influences noise for different surface specifications.
- Part II
  Explore how construction parameters affect $L_{CPX}$ and final surface properties (texture and thickness).
- Part III
  Investigate methodologies for directly measuring porosity attributes such as void content, air flow resistance, and absorption.

# Part I Texture

## 1 Introduction

Texture strongly influences tyre/road noise. Figure 2 shows a sample of a two-dimensional surface profile for a porous asphalt surface captured using an SLP. The profile accurately captures the top surface but cannot adequately describe sub-surface voids.

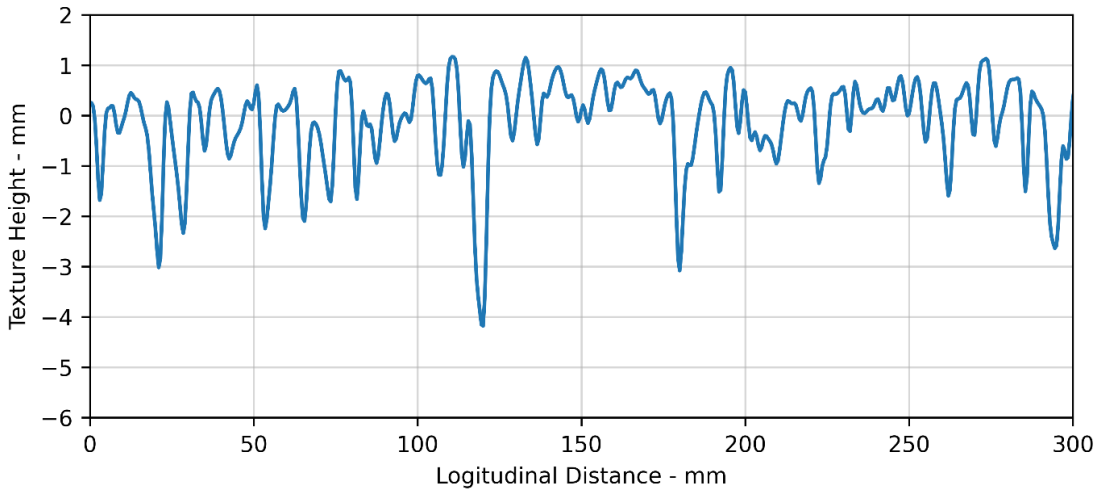


**Figure 2: Example of a 2-D surface profile for PA7 on CNC.**

At present, the primary metric for characterising texture for chipseal and asphaltic surfaces is the mean profile depth (MPD) (ISO 13473-1:2019). MPD only considers the surface profile and not the interaction with the tyre. MPD has no exclusion for surface voids, which limits its physical meaning when used on porous surfaces.

While there have been multiple studies exploring the texture of chipseal (Clapp, Eberhart, & Kelley, 1988) (Meier, van Blokland, & Descornet, 1992) (Fong, 1998), there has been limited research of asphaltic surfaces it their relationship with noise. The studies highlight the need to consider not only the surface profile, but the interaction between the profile and a specific tyre; this has led to the development of envelopment models. Envelopment models predict how the tyre is deformed by the surface texture; these can then be used to predict surface performance properties such as skid resistance and noise.

This study aimed to implement an existing envelopment model on four porous asphalt surfaces and explore the relationships between the resulting enveloped profiles and tyre/road noise.

# 2 Envelopment Model

The Indenter model described in (Goubert & Sandberg, 2018) was employed for the present analysis. The enveloped profile is identified by calculating a constant two-dimensional area of indentation into the tyre as it moves along a given texture profile. For a given tyre footprint length (e.g., 128 mm) a horizontal line is drawn across the local maximum texture height. The line is lowered until the fixed indentation area is reached. See (Goubert & Sandberg, 2018) for a full description of the model.

The following steps were taken to implement the Indenter model on the profiles measured longitudinally in the wheel path using the SLP.

1. The SLP profiles were processed following the methodology described in ISO 13473-1:2019 using the CAPTIF-SLP Python package (Bull J. , 2023).
2. Missing points were either removed (external) or interpolated (internal).
3. A Butterworth band-pass filter was applied with a range of 2.4 to 176.4 mm (from ISO 13473)
4. The Indenter model was applied with the following parameters:
5. Indentation area = 30 mm2
6. Vertical resolution = 0.01 mm
7. Longitudinal resolution = 2 mm
8. Tyre footprint length = 128 mm (sourced from (Sandberg, Goubert, & Vieira, New Measures for Characterization of Negative Surface Textures, 2018))
9. The enveloped profiles were then passed through a second Butterworth bandpass filter with a range of 2.4 to 100 mm.

The applied methodology deviated from that described in (Goubert & Sandberg, 2018) in the slope removal and longitudinal steps. The authors proposed splitting the profile into tyre footprint lengths and removing the slope from each segment. For the present analysis, the longer wavelengths were removed using the bandpass filter and the tyre footprint was incremented along the profile at the longitudinal resolution.

The modified Indenter model was applied to 90 SLP profiles across four surface types on CNC. The quantities of samples by surface type are shown in Table 1. Examples of the enveloped profiles for four surfaces are shown in Figure 3. The SLP and CPX measurements were conducted in March 2023.

**Table 1: Number of SLP profiles per surface type.**

| Surface | Carriageway | Samples |
|---|---|---|
| PA7 LV | NB | 15 |
| PA7 HS | NB | 17 |
| PA7 | NB | 24 |
| | SB | 16 |
| PA10 | SB | 18 |

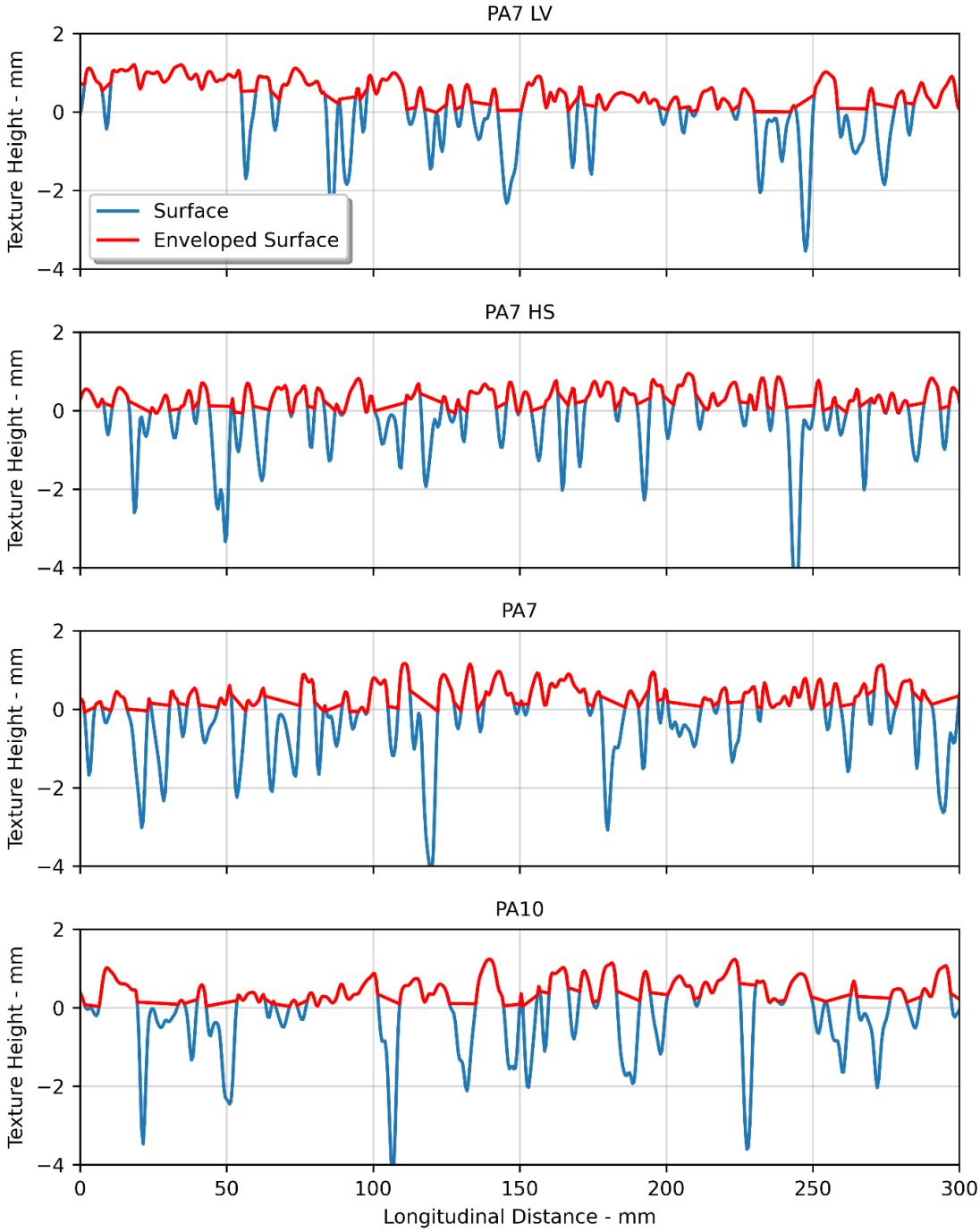


**Figure 3: Examples of enveloped profiles for four surface types on CNC.**

While a 30 mm² indentation area was selected based on its correlation with noise, it differs significantly from the values used in (Goubert & Sandberg, 2018), where typically less than 10 mm² was used for simplified machined test surfaces. It is hypothesised that the indentation area is a function of the texture, however updates to account for this would result in a significantly more complex model. The model also does not consider the non-uniformity of the load at the interface between the tyre and road. Additionally, accounting for the tread pattern of the tyre may also prove to be beneficial.

## 2.1 Metrics and Transformations

To test for correlations with surface properties (i.e., texture and thickness) and noise, multiple metrics were calculated on the enveloped profiles. The longitudinal data was also transformed into the frequency domain. The metrics and transformations are described in Table 2 with a supporting diagram in Figure 4.

**Table 2: Descriptions of metrics and transformations on enveloped profiles.**

| Metric | Description |
|---|---|
| Indent depth | For each increment of the tyre footprint along a profile, the indentation depth, in mm, was calculated. It is the vertical distance between the maximum profile height and the deepest point enveloped by the tyre (indent depth). The median value was calculated for each SLP profile. |
| RMS | The RMS amplitude, in mm, for the enveloped profile, centred about the mean envelopment depth. |
| Texture drainage area (TDA) | The area below the enveloped profile that is available for water drainage and air dispersion; this area does not include sub-surface voids. The units are drainage area per metre ($mm^2$/ m). This metric was proposed in (Sandberg, Goubert, & Vieira, New Measures for Characterization of Negative Surface Textures, 2018). |
| Texture wavelength | The texture wavelengths, in mm, were calculated by passing the longitudinal enveloped profile through a Fourier transform and taking the inverse of the frequency to return wavelength. |
| Spectral density of tyre/texture impact | Welch's method was used to calculate the spectral density of the enveloped profiles. The impact/excitation frequency was calculated from a fixed speed of 80 km/h. The resulting units were $mm^2$/Hz. |

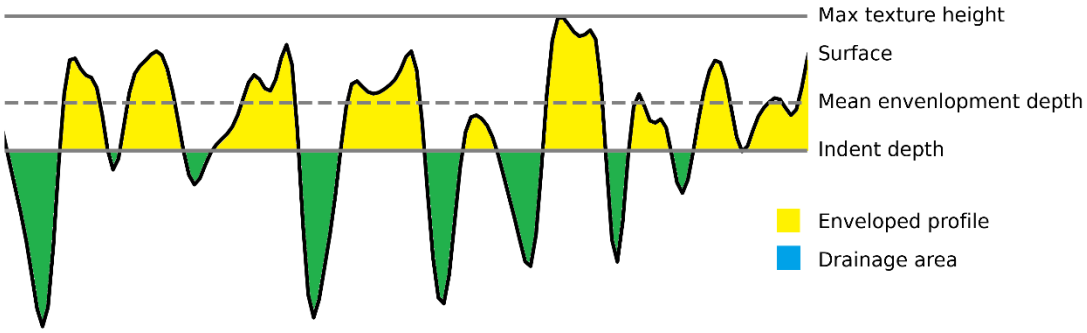


**Figure 4: Enveloped profile metrics diagram.**

# 3 Results and Discussion

Boxplots of the indent depth, RMS, TDA, and (non-enveloped) MPD are shown in Figure 5 for four surface types. The ranking and approximate relative magnitudes are similar for all the metrics with the following order from highest to lowest texture: PA10, PA7, PA7 LV, and PA7 HS.

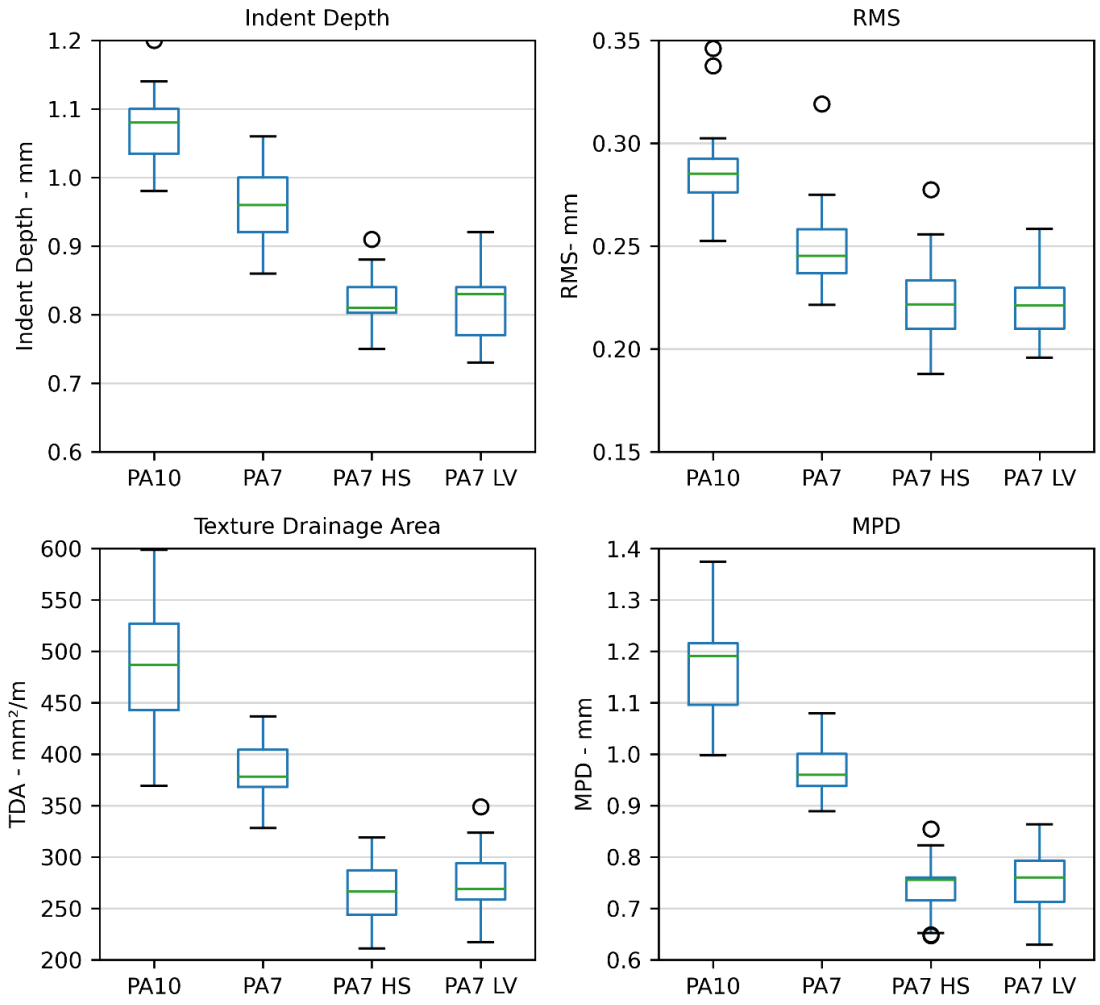


**Figure 5: Boxplots of indent depth, RMS, TDA, and MPD for PA10, PA7, PA7 HS, and PA7 LV on CNC.**

The mean texture wavelengths for each surface type are shown in Figure 6. For a single SLP profile it was common to be able to discern prominent wavelengths in the 20-40 mm range, however when the mean is taken for each surface type no strong peaks were present. Between the four surface types, the primary difference was in the mean amplitude, which is captured within the RMS metric.

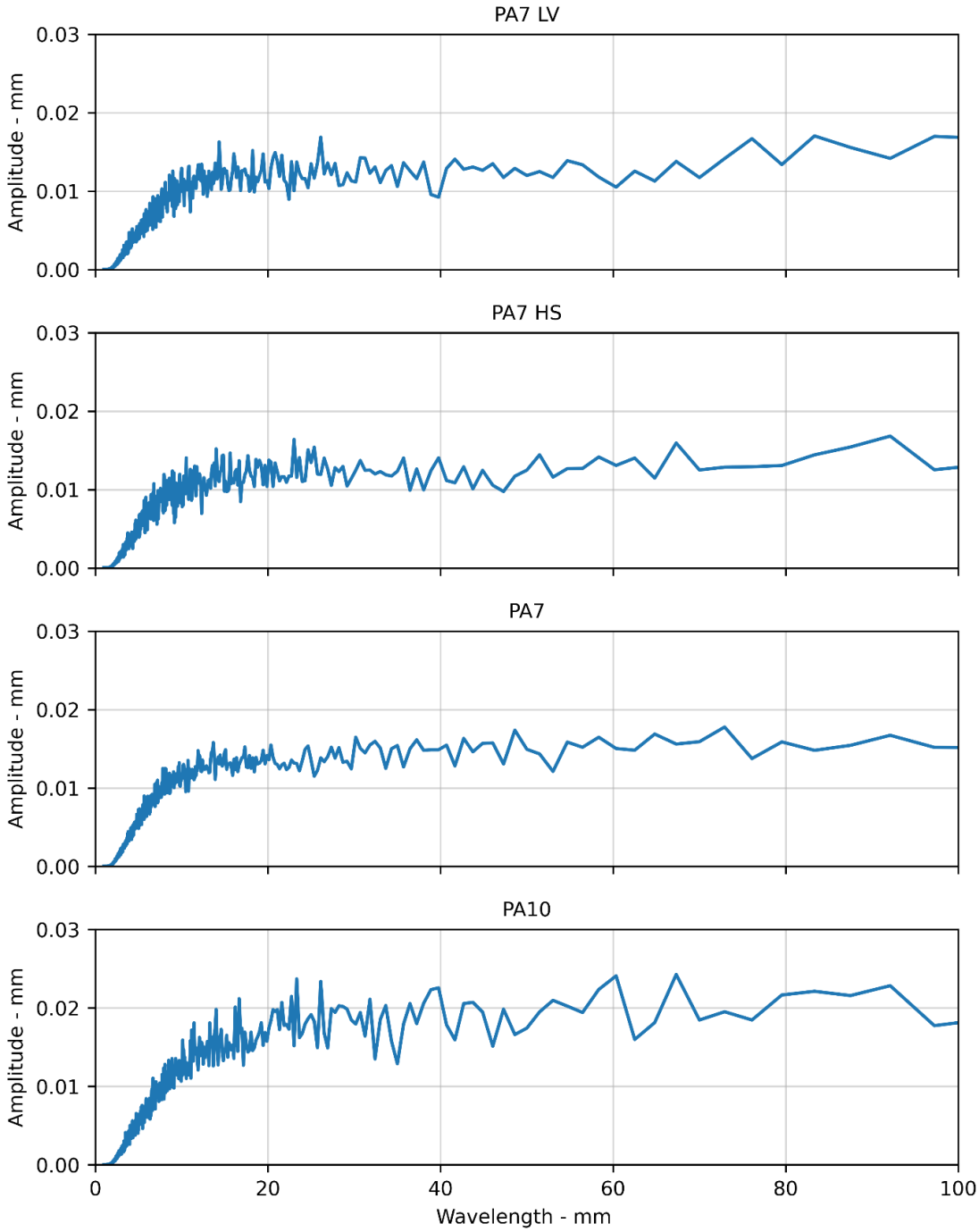


**Figure 6: Mean wavelengths and amplitudes for surfaces on CNC.**

The overall $L_{CPX}$ for 4 m segments are plotted against indent depth, TDA, RMS, and MPD in Figure 7. All metrics had statistically valid ($p < 0.05$) positive correlations with the overall level. Indent depth, TDA, and MPD had the strongest $R^2$ values (0.46).

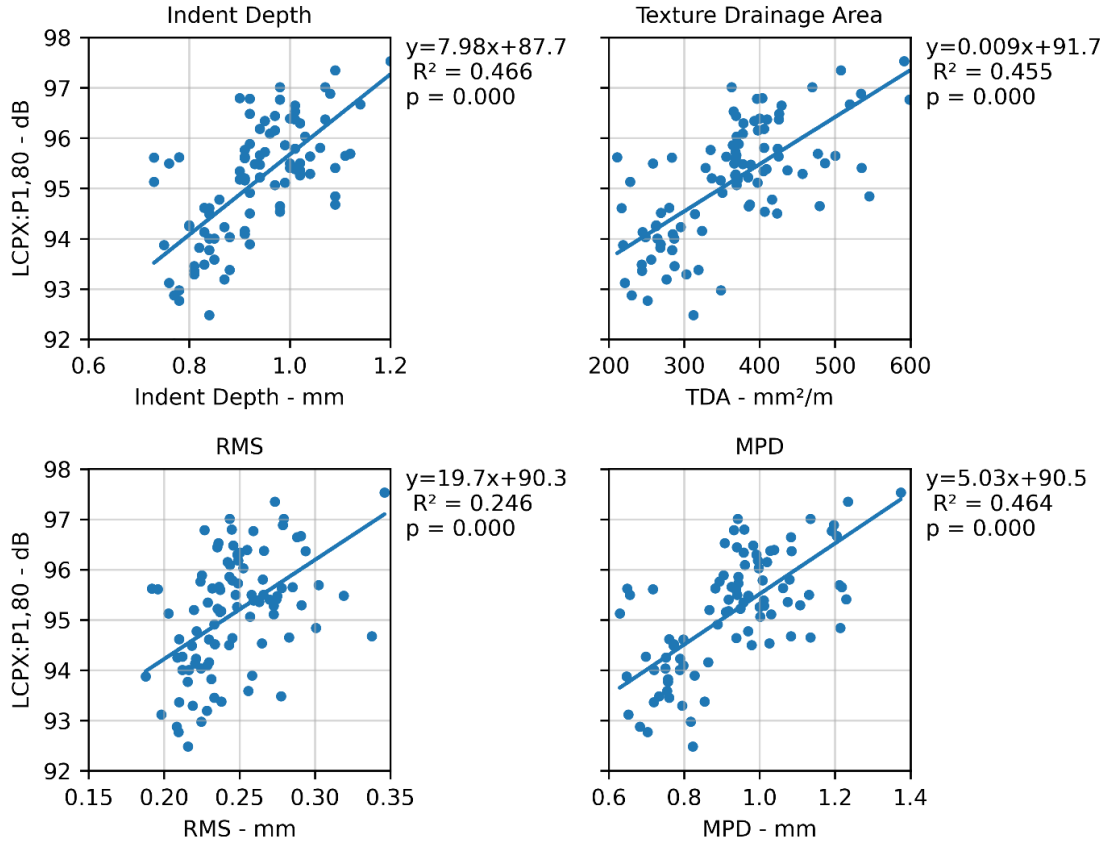


**Figure 7: Scatter plots of $L_{CPX}$ and indent depth, TDA, RMS, and MPD for all surface types.**

Prior analysis (Bell, 2023) has shown that texture has a frequency-dependent effect on $L_{CPX}$. The correlations between indent depth and $L_{CPX}$ are shown in Figure 8 for each one-third octave band. The resulting correlations were similar for RMS, TDA, and MPD (see Figure 21 to Figure 23). $L_{CPX}$ was positively correlated with indent depth up to 1,000 Hz, and negatively correlated in the 1,600, 4,000, and 5,000 Hz bands. The $R^2$ values exceeded 0.7 in the 500 and 630 Hz bands.

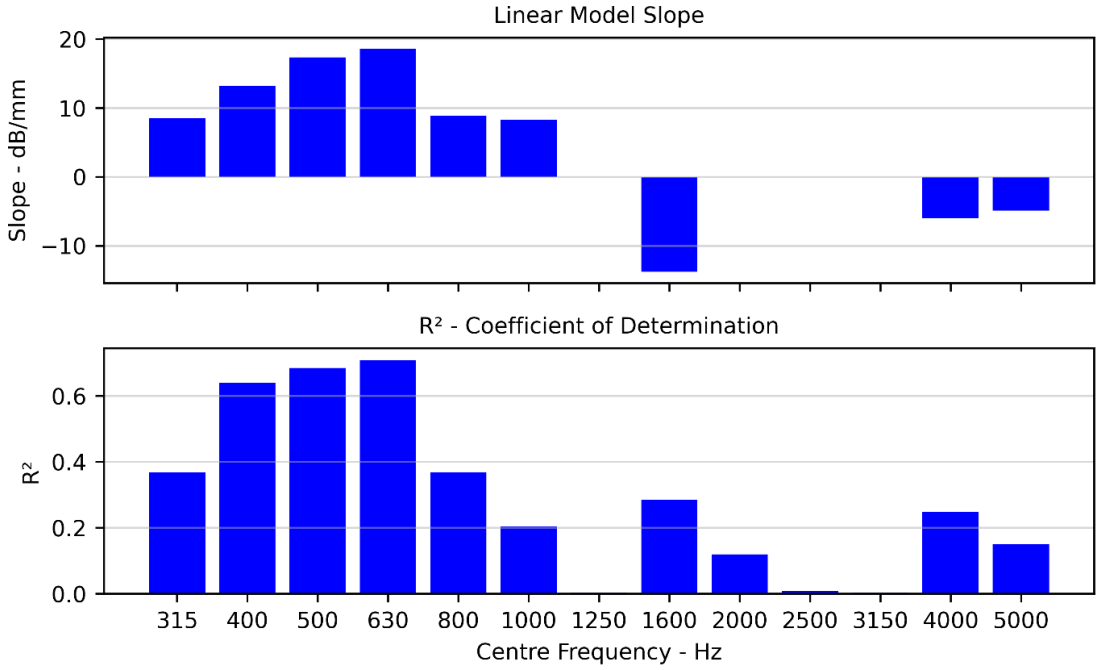


**Figure 8: Correlations and $R^2$ values between one-third octave band levels and indentation depth for PA7 LV, PA7 HS, PA7, and PA10 on CNC.**

The one-third octave band $L_{CPX}$ and enveloped texture spectral density are shown in Figure 9. It should be noted that the $L_{CPX}$ has had the A-weighting removed. The spectral power had a comparable low-frequency (<1,000 Hz) ranking to the $L_{CPX}$ levels. The spectral density showed that most of the texture power is below 1,000 Hz, which aligns with the correlations observed in Figure 23 for MPD versus $L_{CPX}$.

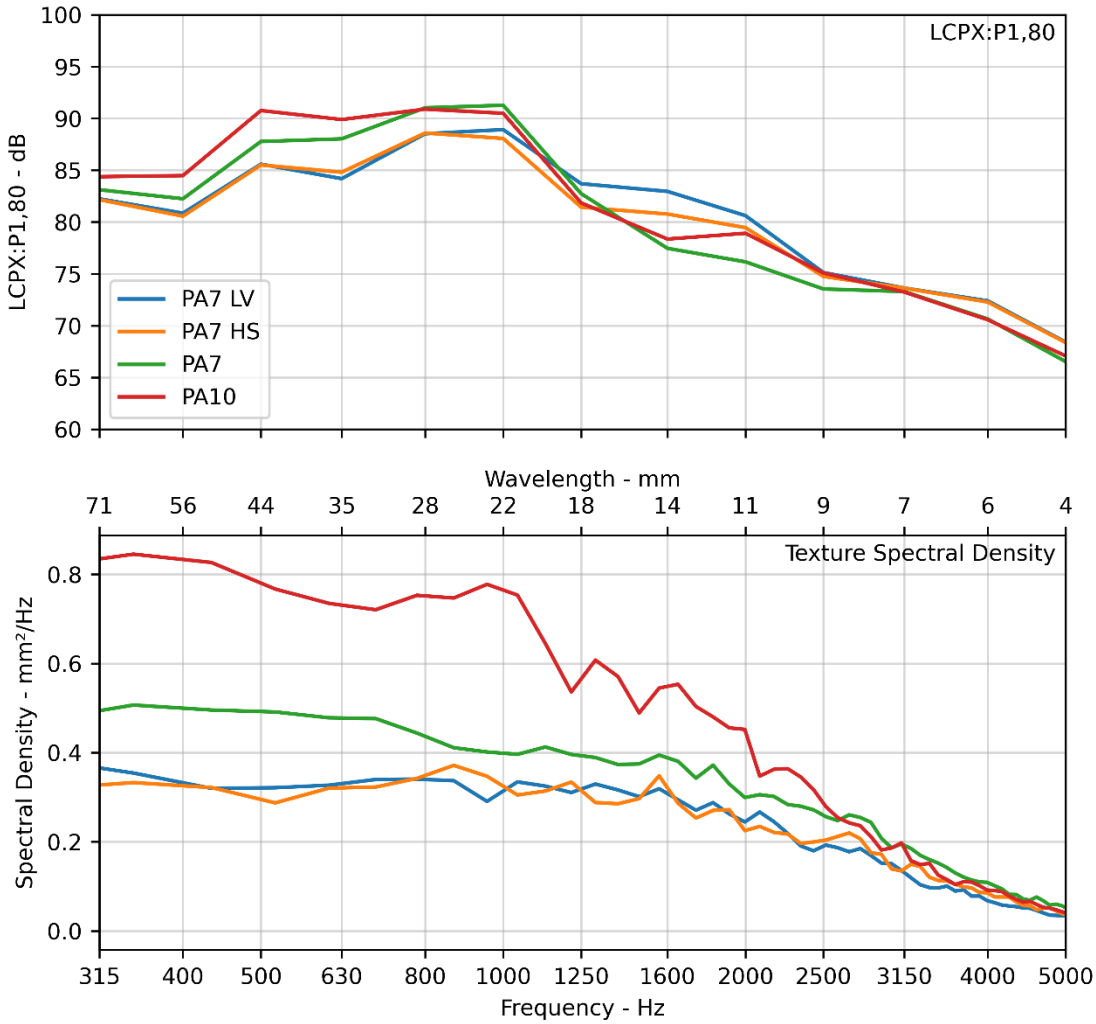


**Figure 9: One-third octave band $L_{CPX}$ and texture spectral density for PA7 LV, PA7 HS, PA7, and PA10 on CNC.**

Indent depth, TDA, and RMS are shown as a function of MPD in Figure 10. All metrics exhibited positive correlations with MPD. While MPD is unlikely to be the underlying metric that affects noise, it is strongly correlated with key metrics from the enveloped profile; this finding supports the ongoing use of MPD for the characterisation of surface texture for porous asphalt.

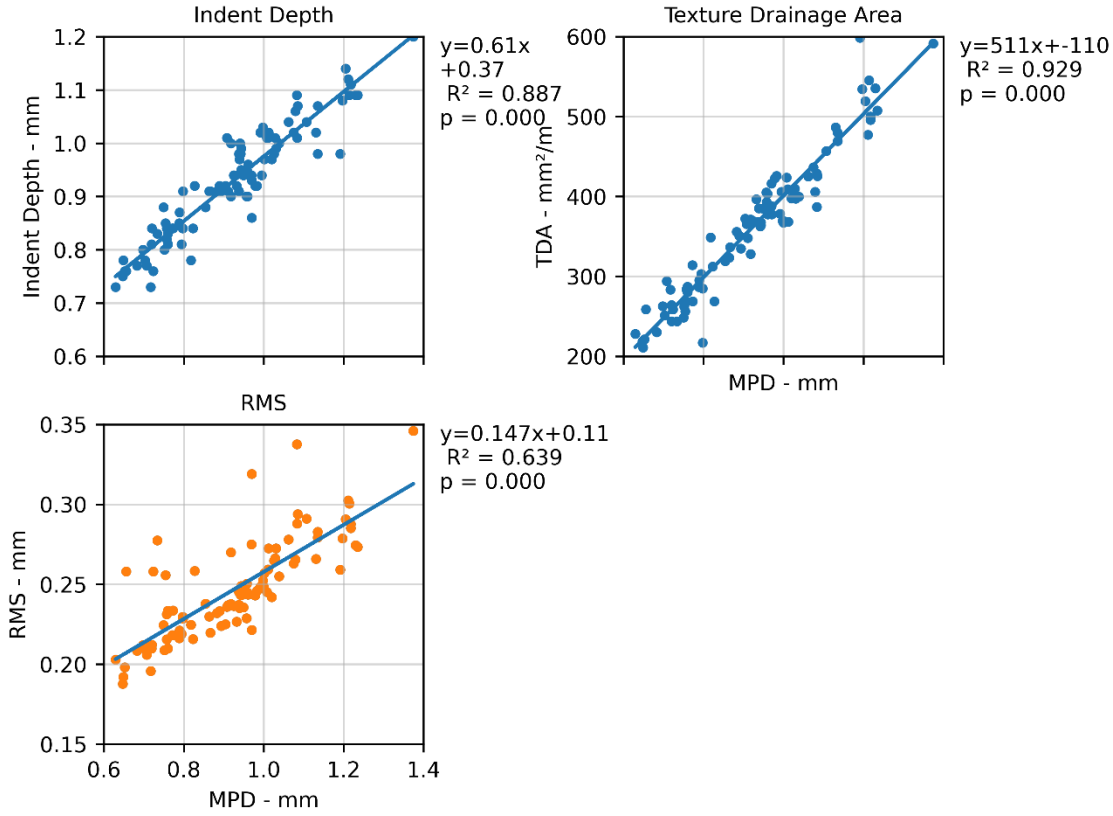


**Figure 10: Scatter plots of MPD and indent depth, TDA, and RMS for all surface types.**

Analysis of the enveloped texture potentially offers insight into the underlying reason for the quieter $L_{CPX}$ levels (relative to PA7) of the PA7 LV and PA7 HS on CNC. Across all metrics, the lower void surfaces showed lesser levels relative to PA7 and PA10. The spectral density indicated that there is less textural power exciting the tyre.

All experimental results are for a P1 tyre. There may be noise-related effects that were not accurately captured. It is recommended that a future investigation explores the influence of texture on a tyre that is more typical of the fleet.

# 4 Future Investigations

- Optimise envelopment model parameters to improve correlations.
- Measure transverse profiles and compare the wavelengths and PSD to confirm the suitability of the orientation of the CPX laser.
- Explore texture effects for the P1 tyre compared to a typical fleet tyre (e.g., Super Cat).
- Integrate MPD into CPX data processing.
- Analyse extended sections of CNC and CSM2 with continuous texture and thickness.
- Analyse chipseal surfaces with envelopment models using either SLP or CPX laser data.

# 5 Conclusions

Previous investigations have shown that texture has a significant influence on tyre/road noise. High resolution SLP profiles for four samples of asphaltic surfaces were analysed. The modified Indenter envelopment model was utilised to estimate the portion of the surface profile that is interacting with the tyre.

Multiple metrics were identified for the enveloped profiles and their predictive capabilities with noise were analysed. The indent depth, TDA, and RMS all showed significant correlations with noise. Analysis of the spectral content of the enveloped profile offered insight into the excitation frequency and amplitude, which may explain the relatively low $L_{CPX}$ levels for the PA7 LV and PA7 HS surfaces.

All the metrics had strong correlations with MPD, which supports its use in future road noise research for porous asphalt.

# Part II Construction

## 1 Introduction

A previous investigation demonstrated that over 70% of the longitudinal variation in tyre/road noise for porous asphalt on CNC and CSM2 was due to changes in thickness and texture (Bell, 2023). It is not presently known what the root-cause of variations in thickness and texture are, and what is the cause of the residual 30%. It was hypothesised that construction parameters and techniques influence the final surface parameters. Construction parameters were explored previously for WBB (Bull J. , 2019), however no significant correlations were observed in the collected data.

The construction of the porous asphalt surfaces on CNC in 2022 was monitored; this included GPS tracking of the paver and primary roller, and temperature logging of the paver outlet.

This study aimed to explore correlations between construction parameters, surface properties (i.e., texture and thickness), and noise.

The data was collected solely for the purpose of conducting retrospective analysis. The primary objective was not to examine surface properties unrelated to sound. Rather, this analysis was taken as an opportunity to ascertain whether the inherent fluctuations in construction procedures had any noteworthy impact on tire/road noise. During the analysis, relationships were established between construction metrics and noise, thickness, and texture. It is likely that other properties are more suited for this opportunistic investigation (e.g., void content), but these were not available at the time of analysis.

## 2 Methodology

This section describes the available data, processing, and calculations of key metrics. A description of the measurement methods and raw data can be found in (Wareing, Christchurch Northern Corridor - 2022 Trial Site Preliminary Investigations). A description of the CPX measurements can be found in (Wareing, Canterbury Road Surface Noise 2022 Measurement Summary).

### 2.1 Trial Sections

Monitoring was undertaken across four paving shifts. The monitored surfaces, nominal specifications, locations, and lengths are shown in Table 3. A map of the CNC trial sections is shown in Figure 29. All surfaces had a nominal thickness of 30 mm.

**Table 3. Nominal surface parameters for each surface type.**

| Surface | NB/SB | Lane | Length* m | Voids - % | Surfacing Date** |
|---|---|---|---|---|---|
| SMA7 | SB | 1 | 424 | 2-6 | 27/2/2022 |
| | | 2 | | | 28/2/2022 |
| PA7 LV | NB | 1 | 360 | 8-10 | 24/2/2022 |
| | | 2 | | | 25/2/2022 |
| PA7 HS | NB | 1 | 320 | 12-16 | 24/2/2022 |
| | | 2 | | | 25/2/2022 |
| PA7 | NB | 1 | 1,788 | 20-25 | 24/2/2022 |
| | | 2 | | | 25/2/2022 |
| | SB | 1 | 1,668 | | 27/2/2022 |
| | | 2 | | | 28/2/2022 |
| PA10 | SB | 1 | 376 | 20-25 | 27/2/2022 |
| | | 2 | | | 28/2/2022 |

*Lengths are after the transitions have been removed.

**Surfacing date is at the start of the shift.

## 2.2 Data

Table 4 shows the data sets used for the analysis and measurement dates.

**Table 4. Data sets and measurement dates.**

| Parameter | Data | Measurement Date |
|---|---|---|
| Tyre/road noise | Overall and one third octave $L_{CPX:P1,80}$ | Jun 2022 |
| As-built thickness | Paving shift records (trace sheets) | - |
| | MIT-SCAN thickness measurements | Mar 2022 |
| Macrotexture | Stationary laser profilometer | Mar 2023 |
| | Road Science Hawkeye | Apr 2022 |
| Nominal surface properties | CAPTIF surface properties database | - |
| Construction parameters | Paver location | Feb 2022 |
| | Roller location | |
| | Paver outlet temperature | |
| | QA trace sheets | - |

## 2.3 Metrics

The collected data was processed to calculate the metrics described below. All data was combined into 4 m longitudinal segments. The metrics calculated for the paver are described in Table 5. The metrics calculated for the roller are described in Table 6.

**Table 5. Paver metrics.**

| Metric | Description |
|---|---|
| Paver speed (max/mean)<br>m/s | Calculated from the mean speed between the adjacent points – not the recorded GPS speed.<br>Calculated the mean and max values for each segment. |
| Paving temperature (min/mean/max)<br>°C | The min/mean/max temperatures were recorded for six discrete transverse boxes at the outlet of the paver. Only boxes 2-4 were included in the analysis as 1, 5, and 6 overlapped with the edge of the paved surface. The following was calculated:<br>• Minimum transverse temperature.<br>• Mean transverse temperature.<br>• Maximum transverse temperature.<br>Measurements were discarded if the paver stopped within a segment. After a stoppage, measurements were discarded until the temperature field of view was on "hot" asphalt (i.e., not on the surface between the screed and the temperature measurement). |
| Paver stopped<br>m/s | The paver was deemed to be stopped if the speed was below 0.02 m/s. The threshold was determined from the speed histogram.<br>The segment was tagged as having a stoppage event and the duration was calculated. |
| Paving width<br>m | Directly recorded on QA trace sheets. |
| Asphalt load length<br>m | Directly recorded on QA trace sheets. |

**Table 6. Roller metrics.**

| Metric | Description and Calculation |
|---|---|
| Roller speed (mean/max)<br>m/s | Calculated from the mean speed between the adjacent points – not the recorded GPS speed.<br>Calculated the mean and max values for each segment. |
| Roller stopped<br>sec | The roller was determined to be stopped if the speed was below 0.1 m/s. The threshold was determined from the speed histogram.<br>The segment was tagged as having a stoppage event and the duration was calculated. |
| Roller direction change<br>- | The roller was deemed to have changed direction if there was a local change in chainage with a height of 10 seconds (i.e., the roller reversed direction for at least 10 seconds). |
| Roller passes<br>- | The mean number of passes through the mid-point of a segment. To calculate the mean number of passes the gross number is divided by two (forward + backwards pass) and divided by the local paving width then multiplied by the roller width (1.68 m). |
| Rolling length<br>m | The rolling length is the distance that is continuously rolled in one direction (i.e., distance between each direction change). |
| Time between paving and rolling<br>min | The difference between the paver and roller both entering the same segment. |

## 2.4 Dependent Variables

The 10 construction parameters were correlated with the 36 available dependent variables, these included:

- Left and right $L_{CPX}$:
  - Overall
  - One-third octave bands
- Texture:
  - $MPD_{HE}$ (measured using Road Science Hawkeye)
  - $MPD_{SLP}$ (measured using CAPTIF SLP)
  - RMS
  - TDA
  - Indent depth
- Thickness

Potentially critical parameters that were not available at the time of analysis were void content, absorption, and air flow permeability.

When a correlation between $L_{CPX}$ and a construction parameter was identified, the corresponding surface property change is hypothesised based on the frequencies that were affected.

## 2.5 Analysis Method

The below steps were followed for each surface type:

- Construction metrics were plotted longitudinally for each surface type.
- Scatter plots were created for independent variables and the dependent variables (e.g., overall $L_{CPX}$, versus paver speed).
- To provide an indication of the likely cause of variations in the dependent variables, they were converted from the length to the frequency/wavelength domain. For example, if $L_{CPX}$ had a longitudinal wavelength that matched the asphalt load length, this may have indicated a load-to-load temperature effect.
- Correlations were tested by calculating the linear regression statistics for all independent versus all dependent variables. In addition, all pairings of independent variables were passed into a multi-variable linear regression model with all dependent variables. Where more than two independent variables were found to have valid correlations with the same dependent variable, the multi-variable model was expanded. Where there was co-linearity between predictor variables for a multi-variable regression, the variable that resulted in the greatest $R^2$ was maintained and the others discarded.

A full set of outputs from the analysis are shown in Appendix A – Additional Data.

# 3 Results and Discussion

## 3.1 Overall Metric Ranges

Boxplots of the mean $L_{CPX}$, paver speed, paving temperature, time between paving and rolling, roller speed, and roller passes are shown in Figure 11 to Figure 16. All results are separated into surface type, lane (1/2), and carriageway (NB/SB). Note that the PA7 is present in both the NB and SB carriageways.

The $L_{CPX}$ varies significantly between surface types with lane 2 (left or slow lane) having a greater relative level. The inter and intra-surface variations in $L_{CPX}$ were explored further in (Bell, 2023).

The paving speed was relatively consistent (~0.1-0.2 m/s) across all surfaces. The consistent paver speed was likely able to be maintained due to the use of an MTV. The narrow range of speed limited the ability to explore the influence of this parameter.

The outlet temperature of the paver was captured for lane 2 on both carriageways. Within the set of porous surfaces, the PA7 LV had a relatively low paving temperature, with a mean minimum temperature of 86°C, compared to 98 °C and 105 °C for PA7 and PA7 HS, respectively.

There was a large range (2 to 20 mins) in the time between paving and the first roller pass. Some variation can be attributed to the roller speed, which can be seen between lane 1 and 2 for the NB carriageway where a higher mean roller speed was paired with a reduction in time to rolling. The roller speed varied between 1 and 2 m/s, with an increase of 0.2 m/s between lane 1 and 2 on the NB carriageway – the cause of the increase is unknown. The mean number of passes ranged from one to five across all surfaces.

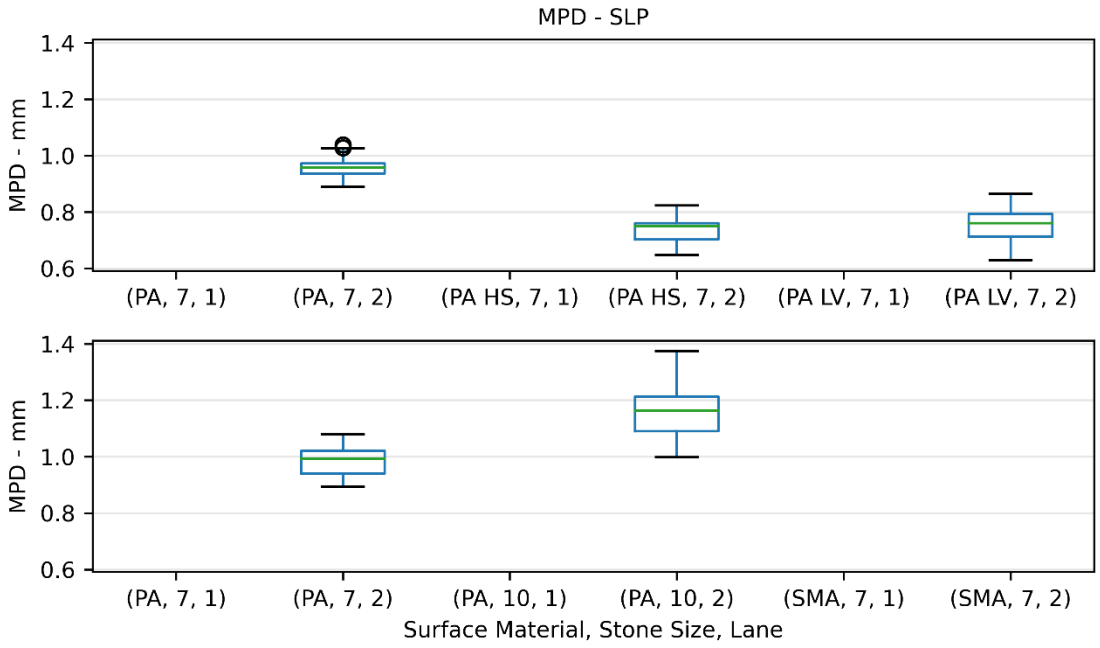


**Figure 11: Boxplots of $L_{CPX}$ for all surface types on CNC.**

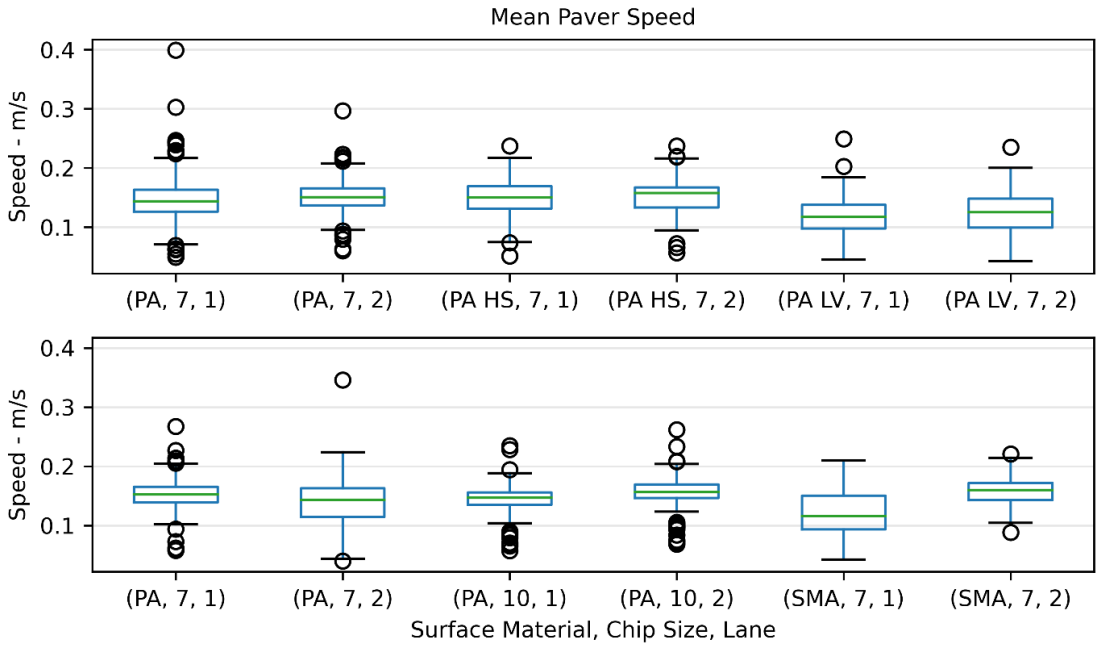


**Figure 12: Boxplots of mean paver speed for all surface types on CNC.**

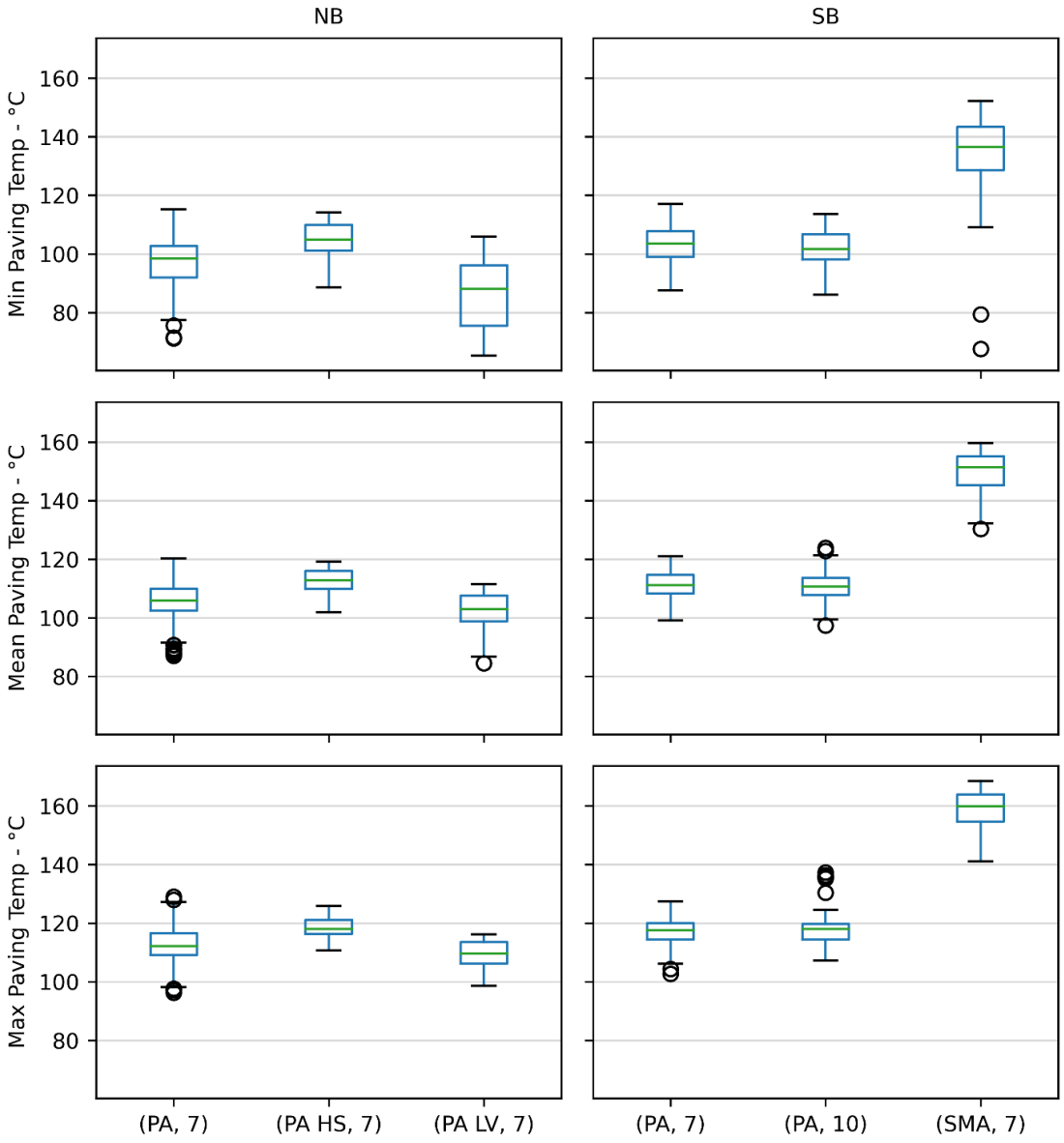


**Figure 13: Boxplots of paving temperature for lane 2 on all surface types on CNC.**

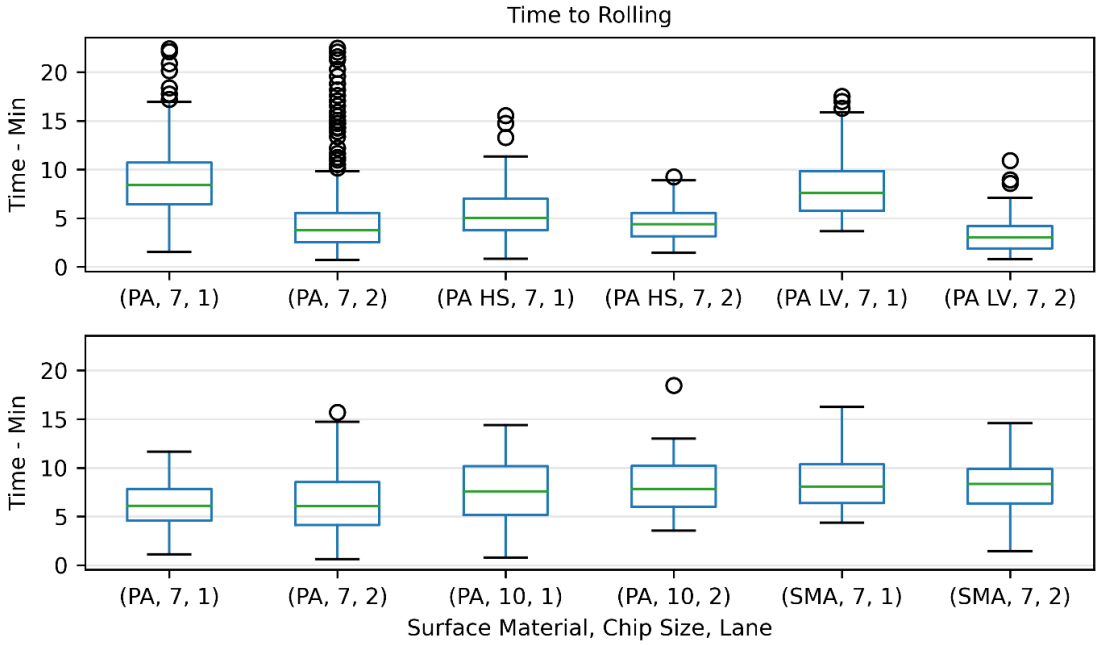


**Figure 14: Boxplots of time between paving and rolling for all surface types on CNC.**

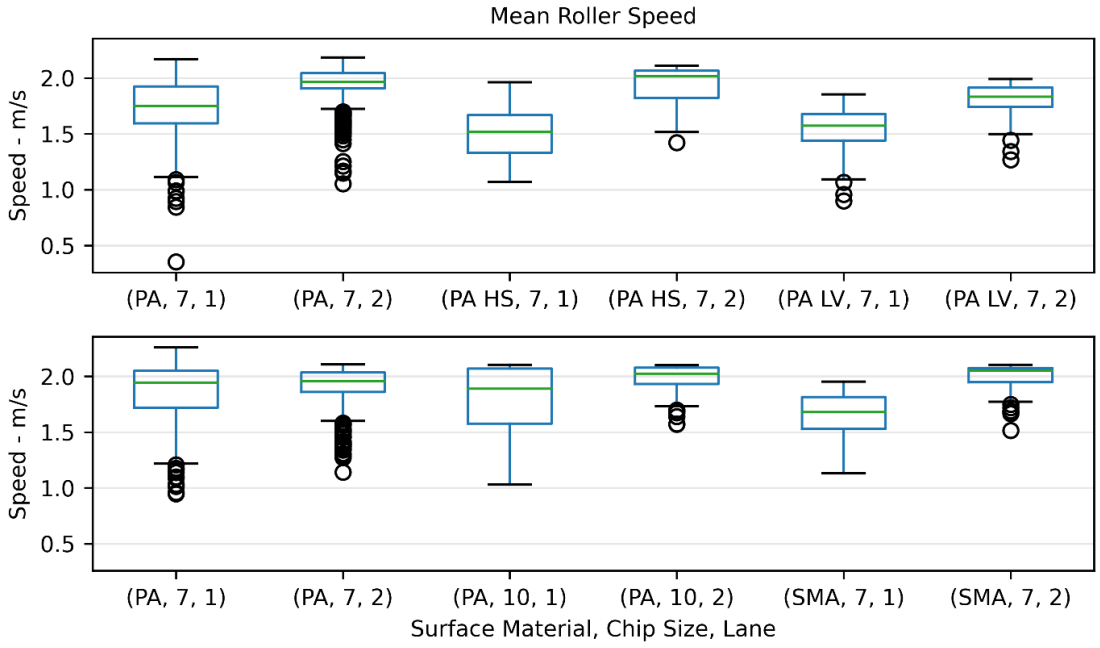


**Figure 15: Boxplots of mean roller speed for all surface types on CNC.**

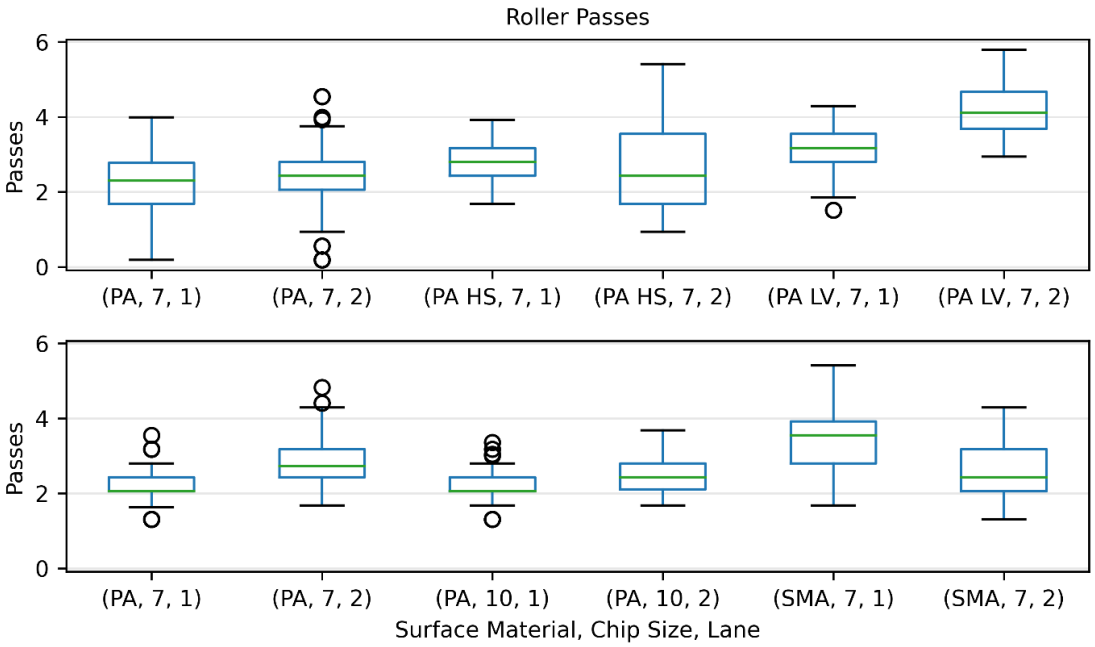


**Figure 16: Boxplots of roller passes for all surface types on CNC.**

## 3.2 Correlations

All pairings of independent and dependent variables were tested for correlations. Only valid and significant correlations are presented and discussed in this section. The criteria were set to a probability (p-value) less than 0.05 and $R^2$ greater than 0.2. The relationships between construction parameters and surface properties (thickness and texture) are presented. The direct effect of construction parameters on $L_{CPX}$ is also explored without the intermediate surface property; this was undertaken as the surface has not been completely characterised (e.g., no void content, air flow permeability, etc.).

It is important to note that the sample size for most correlations is very limited and therefore all results must not be over applied without further investigations. The small quantity of local texture and thickness measurements is the most significant present limitation, followed by the relatively short lengths of the trial sections.

### 3.2.1 Texture

The correlations between construction parameters and texture metrics are shown in Table 7. An example of how to interpret the first row is as follows: indentation depth is negatively correlated with roller speed in lane 2 of the PA7 LV section, where 37% of the variance is explained. Where R2 values are grouped, a multi-variable analysis was utilised.

The mean paving temperature was negatively correlated with MPDSLP for the PA7 LV surface only. The PA7 LV had a relatively low paving temperature, which may indicate a minimum threshold where temperature effects texture. It is recommended that this relationship is explored in further detail when continuous texture data is available.

The time between paving and rolling was positively correlated with MPDHE for both SMA7 lanes and lane 1 of the PA7 LV. It is hypothesised that the relationship is driven by the surface temperature at the time of rolling. It is recommended that the rolling temperature alongside time to rolling is explored retrospectively for WBB or on a future surfacing project.

The roller speed was negatively correlated with indent depth and $MPD_{HE}$ for PA7 LV and SMA7. It is hypothesised that the effect of roller speed reduces as the surface temperature decreases, however further data is required to explore this.

The number of roller passes was negatively correlated with MPDHE for lane 1 of the PA7 LV. It is recommended that the relationship between roller passes, and texture is explored further with a larger data set. The exact lane position (i.e., wheel path) should be determined so the local number of roller passes can be established, rather than using the average across the lane.

**Table 7: Correlations between construction parameters and texture.**

| Texture Metric | Variable | +/- | $R^2$ | P-value | N | Surface |
|---|---|---|---|---|---|---|
| Indent depth | Roller speed | - | 0.37 | 0.01 | 16 | PA7 LV L2 |
| $MPD_{HE}$ | Roller passes | - | 0.36 | 0.02 | 90 | PA7 LV L1 |
| | Roller speed | - | | 0.06 | | |
| | Time to rolling | + | | 0.00 | | |
| | Roller speed | - | 0.38 | 0.00 | 106 | SMA7 L1 |
| | Time to rolling | + | | 0.00 | 106 | |
| | Roller speed | - | 0.35 | 0.00 | 103 | SMA7 L2 |
| | Time to rolling | + | | 0.00 | 103 | |
| $MPD_{SLP}$ | Mean temp | - | 0.47 | 0.03 | 10 | PA7 LV L2 |

### 3.2.2 Thickness

The correlations between construction parameters and thickness are shown in Table 8. The analysis of thickness was significantly limited by the small sample size. It is recommended that the analysis is repeated with continuous high-resolution thickness data (this was not available at the time of analysis).

Thickness was positively correlated with the time between paving and rolling and negatively correlated with the paver speed. It is hypothesised that these are secondary correlations with the primary ones being paving and rolling temperature.

**Table 8: Correlations between construction parameters and thickness.**

| Variable | +/- | $R^2$ | P-value | N | Surface |
|---|---|---|---|---|---|
| Time to rolling | + | 0.8 | 0.02 | 9 | SMA7 L1 |
| Paver speed | - | | 0.06 | 9 | |
| Paver speed | - | 0.42 | 0.01 | 16 | PA7 LV L2 |

### 3.2.3 $L_{CPX}$

All correlations between construction parameters and $L_{CPX}$ were considered on a one-third octave basis. The affected frequency range indicates the potential underlying surface property that is being influenced by the construction parameter. For example, texture is known to primarily influence the low-frequency bands (< 1,000 Hz), while absorption affects the mid-frequency bands (~800-1,250 Hz), and air dispersion has a broad-band mid to high frequency (1,000 – 5,000 Hz) influence (Winroth, Hoever, Kropp, & Beckenbauer, 2013).

Figure 17 contains an example of a multi-variable model between paving temperature, roller passes, and the time between paving and rolling for PA7 LV. Using the 1,000 Hz band as an example, approximately 50% of the variance in $L_{CPX}$ is accounted for in positive correlations with the mean temperature and roller passes, and no correlation with time to rolling. The y-axis is the slope of the correlation multiplied by the 95$^{th}$ percentile range of the parameter. For example, paving temperature has a correlation slope of 0.1 dB/K and the 95$^{th}$

percentile range is 25 K within PA7 LV. The resulting predicted range of the mean $L_{CPX}$ due to paving temperature is 2.5 dB in the 1,000 Hz band.

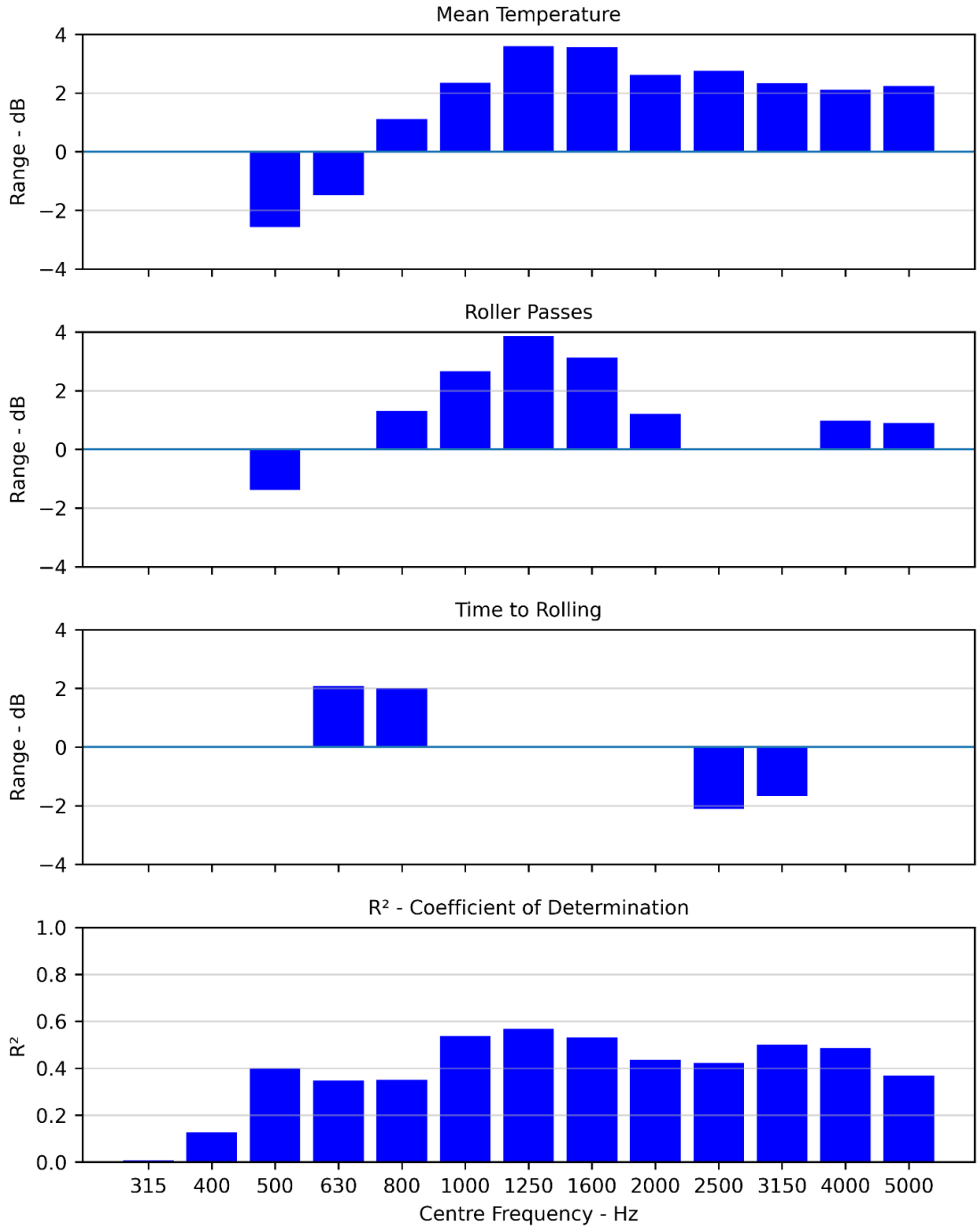


*Range is ± the standard error (95%). Only values with a p-value above 0.05 are shown.*

**Figure 17: Multi-variable model for one-third octave band $L_{CPX}$ levels for PA7 LV lane 2 on CNC.**

All significant correlations ($p < 0.05$) between construction parameters and $L_{CPX}$ are shown in Table 9. The table can be interpreted as follows for the first row. Mean temperature is negatively correlated with the 400 and 500 Hz bands for lane 2 of the PA10, with an estimated mean effect of 3.1 to 3.4 dB. A multi-variable analysis was completed in all instances where multiple construction parameters were considered for the same surface type and lane.

Mean temperature was negatively correlated with low-frequency bands (400-630 Hz) and positively correlated with mid- to high-frequency bands. The negative low-frequency correlations suggested that mean temperature was negatively correlated with texture, which was observed above. The positive mid- to high-frequency correlations may possibly be attributed to absorption and air flow permeability. It is recommended that porosity properties (e.g., air flow permeability, void content, absorption, etc.) are explored further to understand the underlying mechanism being affected by paving temperature.

Roller passes exhibited contradictory correlations between surface types and lanes. The direction of the correlations switched between sample groups. In some instances, low-frequency bands are negatively correlated with roller passes, which implied reducing texture. While in other groups increasing texture was implied. Other surface characteristics (e.g., texture) must be known to understand the influence of the number of passes by the roller. In addition, the surface temperature at the time of rolling and the wheel path must also be known.

Roller speed was negatively correlated with low- to mid-frequencies for lane 2 of the PA7 HS and high frequencies (> 1,600 Hz) for lane 1 of the PA7 HS and PA7 LV. As described above, roller speed was negatively correlated with texture, which is supported by the low-frequency negative correlations. The cause of the high frequency correlation is unknown. It is hypothesised that there is an internal surface property, such as air flow permeability, that is affected by the roller speed. It is recommended that the analysis is repeated when air flow permeability and void content data are available.

The time between paving and rolling was positively correlated with low- to mid-frequency bands, while mid- to high frequency bands were negatively correlated. It is not known why there were opposite correlations for the mid-frequencies; this may have been a combined effect of thickness and texture. It is hypothesised that these correlations were secondary to the primary relationship between the surface temperature during rolling and $L_{CPX}$. It is recommended to retrospectively analyse the rolling temperature for WBB or/and directly measure the surface temperature at the time of rolling on a new surfacing project.

**Table 9: Correlations between construction parameters and $L_{CPX}$.**

| | | $L_{CPX}$ | | |
|---|---|---|---|---|
| Variable | +/- | Frequency - Hz | Range* – dB | Location |
| Mean temp | - | 400, 500 | 3.1 – 3.4 | PA10 L2 |
| | | 500, 630 | 1.5 – 2.6 | PA7 LV L2 |
| | + | 1,000, 1,250 | 1.0 – 1.2 | PA7 HS L2 |
| | | 1,000-5,000 | 2.1 - 3.6 | PA7 LV L2 |
| Roller passes | - | 800 | 3.3 | PA10 L1 |
| | | 500 | 1.4 | PA7 LV L2 |
| | | 1,250-5,000 | 1.1 - 1.4 | PA7 HS L1 |
| | | 400-630 | 2.0 – 3.6 | PA7 HS L2 |
| | + | 800-2000, 4000, 5000 | 1.2 – 4.4 | PA7 LV L2 |
| | | 1,250-5,000 | 1.7 - 5.3 | PA7 HS L2 |
| | | 500 | 2.7 | PA7 LV L1 |
| Roller speed | - | 1,600-5,000 | 1.0 - 1.2 | PA7 HS L1 |
| | | 630-1,000 | 2.1 – 3.8 | PA7 HS L2 |
| | | 1,600-3,150 | 0.8 – 1.0 | PA7 LV L1 |
| Time to rolling | - | 800,1,000 | 6.4 – 7.2 | PA10 L1 |
| | | 1,250-5,000 | 0.8 – 2.6 | PA7 HS L1 |
| | | 1,250-3,150 | 1.5 – 2.7 | PA7 LV L1 |
| | | 2,500, 3,150 | 1.6 – 2.0 | PA7 LV L2 |
| | + | 400, 500, 1,600 | 2.0 – 6.0 | PA10 L1 |
| | | 630 | 2.4 | PA7 HS L1 |
| | | 800, 1,000 | 1.9 – 2.5 | PA7 HS L2 |
| | | 500 | 2.3 | PA7 LV L1 |
| | | 630, 800 | 2.0 – 2.1 | PA7 LV L2 |

$N > 77$, $R^2 > 0.2$, and $p < 0.05$ for all points.
*Range is the overall 95$^{th}$ percentile within the specific surface and lane.

# 4 Future Investigations

The following areas are recommended for further investigation:

- Review the WBB construction data for the effect of rolling temperature on texture and one-third octave band $L_{CPX}$.
- Measure rolling temperature on the next suitable surfacing project.
- Explore the effect of the intra lane position (i.e., wheel path). The GPS accuracy may be a limiting factor.
- Repeat the texture analysis with data from the CPX laser.
- Repeat the analysis with continuous thickness considering wheel path.
- Measure void content, absorption, and air flow permeability and repeat the correlation analysis.

# 5 Conclusions

The roller and paver locations, and paver outlet temperature were measured for five surface types over four separate paving shifts on CNC. Construction metrics were calculated, and their influence was tested against texture, thickness, and noise.

Texture was negatively correlated with paving temperature, roller speed, and roller passes. Texture was positively correlated with the time between paving and rolling. A larger sample size and high-location-accuracy texture measurements must be evaluated to corroborate these findings.

Thickness was negatively correlated with paver speed and positively correlated with the time between paving and rolling. It is hypothesised that the temperature at the time of rolling is the primary relationship, but this could not be confirmed with the available data for CNC.

$L_{CPX}$ had complex frequency-dependent correlations with construction parameters. Correlations were observed between paving temperature, roller speed, roller passes, and time between paving and rolling. Inconsistencies in the correlations were not able to be explained with the existing data.

All results should be considered as indicative due to the limited sample size. Further field measurements of texture and thickness will enable the sample sizes to be increased.

Correlations were tested between 10 independent and 36 dependent variables. There were only a small number of weak correlations. This analysis did not reveal any construction parameters to have a major influence on the longitudinal variation in $L_{CPX}$.

The absence of correlations does not necessarily negate the potential influence of construction processes on both tyre/road noise and the underlying surface properties. This study was carried out utilising the diversities inherent in construction procedures. For a comprehensive investigation into the impact of construction processes on surface properties, a focused parametric study would be better suited. Nonetheless, it's important to clarify that this study was not designed with that objective.

It is recommended that additional surface properties are measured, and the correlation analysis is repeated.

# Part III Porosity Effects

## 1 Introduction

The porosity of a surface can be described through the following:

- Void content: Amount of inter-connected voids open to the atmosphere.
- Void structure: A combination of the shape, size, and layout of the voids

Figure 1 suggests that the surface properties that directly influence $L_{CPX}$ are absorption and air flow permeability.

The absorption of a surface is a function of the thickness, void content, air flow resistance, and void structure (Berengier, Hamet,, & Bar, 1990). The air flow resistance is a function of the other listed parameters. A porous surface has a multi-peaked absorption curve; an indicative curve is shown in Figure 18.

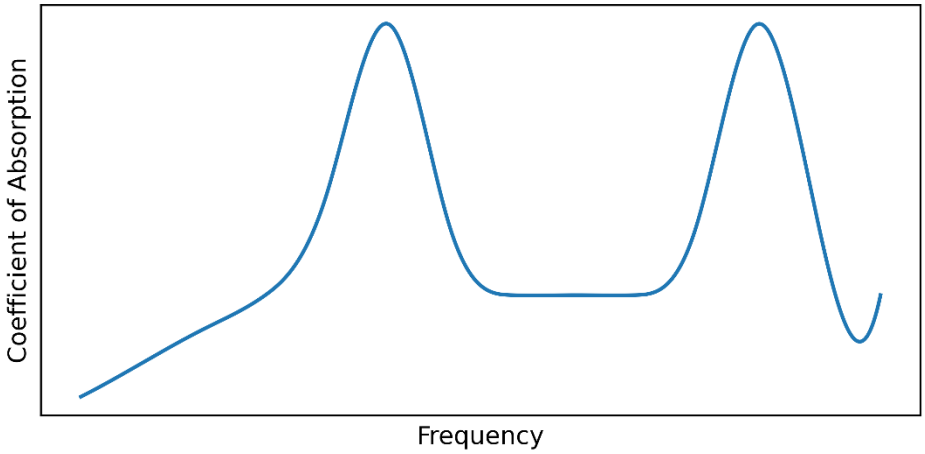


**Figure 18: Form of absorption curve for a porous layer.**

The surface properties have the following theoretical influences on the absorption characteristics.

- Thickness:
  - Peak frequency decreases with increasing thickness.
  - Peak absorption coefficient decreases with increasing thickness.
- Void content
  - Width of absorption peaks increases with increasing void content.
  - Inter-peak absorption increases with increasing void content.
- Air flow resistance
  - Peak absorption decreases with increasing air flow resistance.
  - Inter-peak absorption increases with increasing air flow resistance.
- Void structure (referred to as shape factor):
  - Peak frequency decreases with increasing shape factor.

Void structure/shape factor is not physically defined and is used as an adjustment factor on experimental results.

Air flow permeability describes the ability of the surface to dissipate air being displaced by the tyre as it rolls along the road (also known as "air pumping"). This is a different flow regime (turbulent versus laminar) to the flow induced by acoustic pressure. Air flow permeability is likely a function of void content, void structure, and thickness.

Of the surface properties that influence absorption and air flow permeability, the following might be directly measured: void content, air flow resistance, and thickness. In addition, absorption and air flow permeability can be directly measured. Void structure cannot be viably measured in the field.

It is recommended that methods are explored for measuring absorption, permeability, void content, and thickness. Possible methods are described in this part.

# 2 Methods

Potential methods for measuring surface properties are shown in Table 10. A description of each method is below.

**Table 10: Methods for measuring surface properties.**

| Absorption | Air Flow Permeability | Void Content | Thickness |
|---|---|---|---|
| ISO 13472 -1 Extended Surface Method | Water column | NDM | GPR |
| | In situ air flow permeability | GPR | |
| ISO 13472-2 Impedance Tube Method | | | |

Methods for measuring thickness were extensively reviewed in (McIver & Jackett, 2020) and multiple techniques are presently being employed in New Zealand. The current study is only considering post-surfacing methods that do not require pre-surfacing actions (e.g., placing aluminium disks for the MIT SCAN).

## 2.1 ISO 13472-1 Extended Surface Method

ISO 13472-1 describes a in situ test method for the measurement of the sound absorption coefficient of road surfaces as a function of frequency using free-field propagation. The method measures an area of approximately 3 $m^2$ and encompasses a frequency range of 250 to 4,000 Hz.

A sound source and microphone are located above the surface to be tested. A transfer function is created between the input signal and the output from the microphone. The transfer function considers the sound received directly from the source and that reflected from the surface.

A previous trial of this method was conducted on CNC (Wareing, Christchurch Northern Corridor - 2022 Trial Site Preliminary Investigations). It was found that an adequate signal to noise ratio was not attained, rendering the captured data unusable. A swept sine wave with a duration of 30-seconds was used as an input signal. It was found that the unsteady background noise caused erroneous results.

It is recommended that the measurements are repeated using a maximum-length sequence (MLS) input signal; this will enable significantly shorter measurements
(~1.3 s) and a high number of samples (i.e., > 32).

## 2.2 ISO 13472-2 Impedance Tube Method

ISO 13472-2 describes a in situ test method for the measurement of the sound absorption coefficient of road surfaces as a function of frequency using an impedance tube. This method is intended for use with smooth low-absorption surfaces. The method is described as unreliable if the absorption coefficient exceeds 0.15. The method is complementary to ISO 13472-1, which is suited for surfaces with higher sound absorption coefficients. Both methods should provide comparable results to ISO 10534, which measures the absorption coefficient of core samples using an impedance tube.

It is expected that the absorption coefficient will exceed 0.8 in some frequency bands for porous asphalt (Berengier, Hamet,, & Bar, 1990). Due to the unsuitability of this method for use with surfaces having a sound absorption coefficient greater than 0.15, this method has not been considered further.

## 2.3 In Situ Air Flow Permeability

A laboratory method for measuring the air flow resistance for laminar flow in a porous medium is described in ISO 9053-1:2018 Acoustics – Determination of airflow resistance. The method is limited to extracted core samples and laminar flow, which is not representative of the turbulent flow caused by the rapid displacement of air into the surface by the tyre. In the absence of a standardised method, a possible in situ method is proposed here that more closely represents the air flow induced by a rolling tyre.

Figure 19 contains a schematic of a proposed test apparatus that could be used for the in-situ measurement of air flow permeability. A plenum is placed on the surface of the road and a known air flow rate is passed horizontally through the porous asphalt. Measuring the flow rate and pressure differential allows for the creation of a system curve (see Figure 20 for indicative curves).

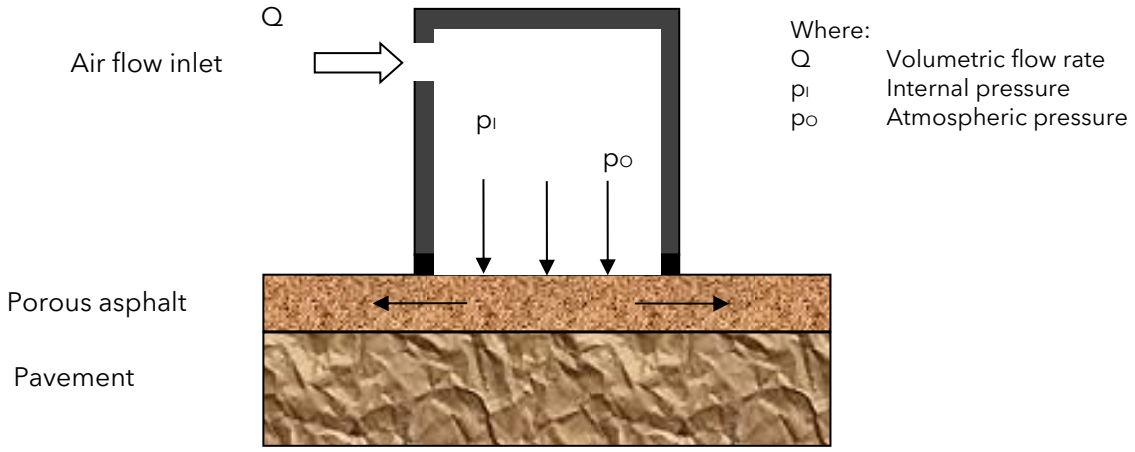


**Figure 19: Schematic of air flow permeability measurement apparatus.**

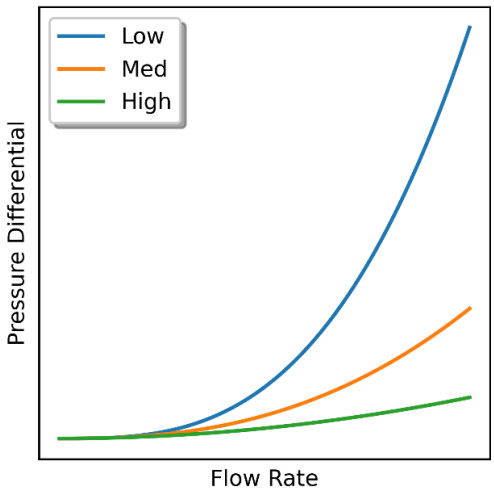


**Figure 20: Example of three system curves for varying air flow permeabilities.**

The intended methodology would be:

1. Place apparatus on the road surface in the wheel path.
2. Apply a known downwards load to achieve suitable sealing.
3. Incrementally increase the air flow rate while measuring the pressure differential.

It is estimated that each measurement would take 1-2 minutes.

The resulting system curves would potentially offer a prediction of the ability of the surface to disperse air and the associated decrease in tyre/road noise due to "air pumping". In addition, relative measurements of a surface over time may indicate "clogging" of the voids.

Limitations and unknowns of the proposed test are:

- While the flow rate may encompass the actual range for a rolling tyre, the inlet flow distribution and any compressibility effects are not being reproduced.
- The results are for a single point on the surface.
- Indicative values are not presently known for flow rates and pressure drop. Additional research must be undertaken to ensure suitable sizing of components (air supply and pressure transducers).
- There will be air leakage between the seal and the road surface, which will be influenced by the macro-texture. The seal design and loading must ensure the resulting system curves are dominated by sub-surface flow.

## 2.4 Water Permeability

The ability of a surface to retain and distribute water is determined by its water permeability. It is expected that the water permeability is directly related to the void content and air flow resistance of the surface and could potentially provide a comparative indication of the air flow permeability.

The water permeability was measured for WBB (Bull J. , 2019). It was found that the method was not practicable for field measurements due to protracted measurement time and the need to fill a significant portion of the voids before a stable measurement could be achieved. The results offered indicative rankings of the surfaces but lacked the resolution to enable correlations for construction parameters and $L_{CPX}$.

It is not recommended that water permeability is considered further for investigating absorption and air dispersion effects of tyre/road noise.

## 2.5 Nuclear Densometer

The nuclear densometer (NDM) is a tool for measuring the density of asphalt surfaces and is commonly used in the construction and maintenance of roads. The methodology is prescribed in AS/NZS 2891. 14.2:2013. The basic principle of the NDM is that the amount of radiation that is absorbed or scattered by the asphalt surface is directly proportional to the density.

The NDM is unable to differentiate between the surface texture and internal voids, which may lead to an overestimation of the void content. Moreover, instead of the interconnected void content that is more pertinent to noise and water drainage, the NDM provides the total void content.

The estimated density measured by the NDM is available for recent projects (CSM2 and CNC). However, the exact locations of the measurements are not known, and the longitudinal resolution is low, which means correlations between construction parameters and noise could not be explored.

It is recommended that two activities are completed with the NDM:

- Conduct measurements on WBB adjacent to the core sampling locations to provide validation of the results and any correction that may be applied for surface texture.
- Conduct measurements on CNC across the thickness measurement points with high location accuracy. Measure at 10 m longitudinal resolution in both left and right wheel paths.

## 2.6 Ground Penetrating Radar

Ground penetrating radar (GPR) is a non-invasive method that employs radar to produce internal images of materials. The technique entails emitting electromagnetic waves into the material and assessing the intensity and delay of the reflected waves. Through interpretation of the data, the thickness and void content can be estimated.

Waka Kotahi have commissioned previous reviews of the GPR method. A review of GPR technology can be found in (McIver & Jackett, 2020). A trial of a GPR was undertaken for WBB (Bull J. , 2019). The trial utilised an air coupled mobile GPR that was traversed along WBB at 80 km/h. The resulting data did not yield any information about the thickness or void content of the asphalt surface. The poor results were attributed to the following:

- The input signal frequency (2.4 GHz) would only allow for resolution of thicknesses greater than 70 mm.
- The air-coupling introduced a variable reflection from the surface and required significant post-processing to remove it.

It is recommended that the utilisation of a ground coupled GPR with a higher frequency input should be reconsidered for measuring thickness and void content. If this approach yields positive outcomes, then a mobile air-coupled unit should be re-evaluated as well.

# 3 Recommendations

It is recommended to undertake the following measurements:

- Absorption: ISO 13472-1: Extended Surface
    - Measure trial sections on CNC.
    - Measure thickness survey sections on CSM2.
- NDM:
    - Measure density at core sample locations on WBB.
    - Measure trial sites on CNC.
- GPR:
    - Use a ground coupled GPR on CNC trial sites.
    - Use an air-coupled GPR on CNC trial sites (only if ground-coupled is successful).
- Air flow permeability:
    - Develop in situ air flow permeability test apparatus.
    - Measure trial sites on CNC.

# 4 References


Bell, G. (2023). *Analysis of Low-Noise Asphaltic Mix Surfaces.* Christchurch, New Zealand: Altissimo Consulting Ltd.

Berengier, M., Hamet,, F., & Bar, P. (1990). *Acoustical properties of porous asphalts: theoretical and environmental aspects.* Transportation Research Record. (1265).

Bull, J. (2019). *Road surface noise research - Porous asphalt variability study.* Christchurch, New Zealand: Altissimo Consulting Ltd.

Bull, J. (2023). *CAPTIF Road Research Centre*. Retrieved from GITHUB: https://github.com/captif-nz

Clapp, T., Eberhart, A. C., & Kelley, C. (1988). Development and Validation of a Method for Approximating Road Surface Texture-Induced Contact Pressure in Tire-Pavement Interaction. *Tire Science and Technology*.

Fong, S. (1998). Tyre Noise Predictions from Computed Road Surface Texture Induced Contact Pressure. *Internoise 98*. Christchurch, New Zealand.

Goubert, L., & Sandberg, U. (2018). Enveloping Texture Profiles for Better Modelling of Rolling Resistance and Acoustic Qualities of Road Pavements. *SURF 2018.* Brisbane, Queensland 2018.

Hamet, J. F. (2004). *Reduction of tire road noise by acoustic absorption: Numerical evaluation of the pass-by noise level reduction using the normal incidence acoustic absorption coefficient.* Bron Cédex - France: Laboratoire Transport et Environnement.

Li, T. (2018). Influencing Parameters on Tire–Pavement Interaction Noise: Review, Experiments, and Design Considerations. *Designs 2, 4*, 38.

McIver, I., & Jackett, R. (2020). *Measurement of asphalt thickness.* Petone, New Zealand: WSP.

Meier, V., van Blokland, A., & Descornet, G. J. (1992). The influence of texture and sound absorption on the noise of porous road surfaces. *SURF 1992.* Berlin, Germany.

Peeters, B., & Kuijpers, A. (2008). The effect of porous road surfaces on radiation and propagation of tyre noise. *Journal of the Acoustical Society of America*, 123(5), 3673-3673.

Sandberg, U., & Ejsmont, J. A. (2002). *Tyre/road noise. Reference Book.*

Sandberg, U., Goubert, L., & Vieira, T. (2018). New Measures for Characterization of Negative Surface Textures. *SURF 2018.* Brisbane, Queensland.

Wareing, R. (2022). Canterbury Road Surface Noise 2022 Measurement Summary.

Wareing, R. (2022). *Christchurch Northern Corridor - 2022 Trial Site Preliminary Investigations.* Christchurch, New Zealand: Altissimo Consulting Ltd.

Winroth, J., Hoever, C., Kropp, W., & Beckenbauer, T. (2013). The contribution of air-pumping to tyre/road noise. *AIA-DAGA 2013*, (pp. 1594-1597).

# Appendix A – Additional Data

## Texture

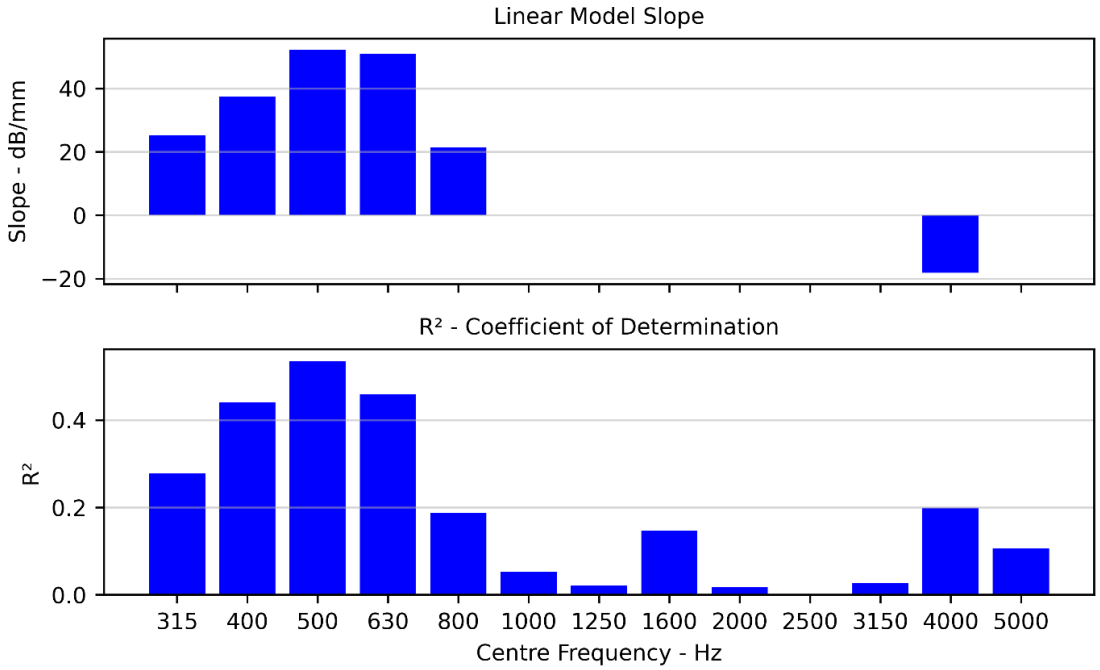


**Figure 21: Correlations and $R^2$ values between one-third octave band levels and enveloped RMS for PA7 LV, PA7 HS, PA7, and PA10 on CNC.**

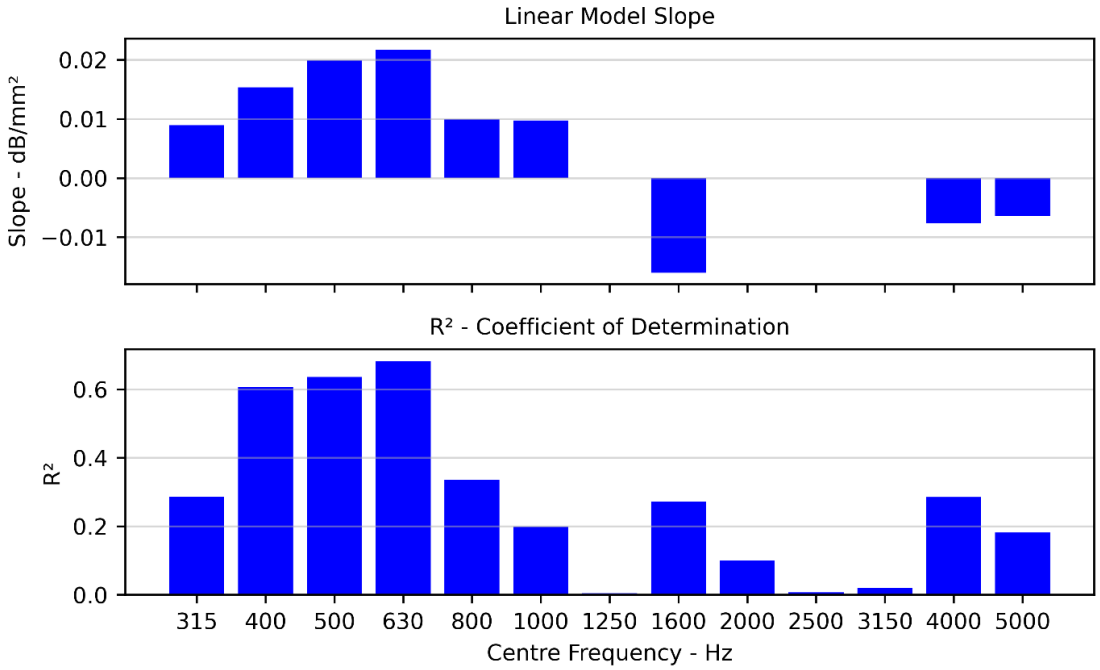


**Figure 22: Correlations and $R^2$ values between one-third octave band levels and TDA for PA7 LV, PA7 HS, PA7, and PA10 on CNC.**

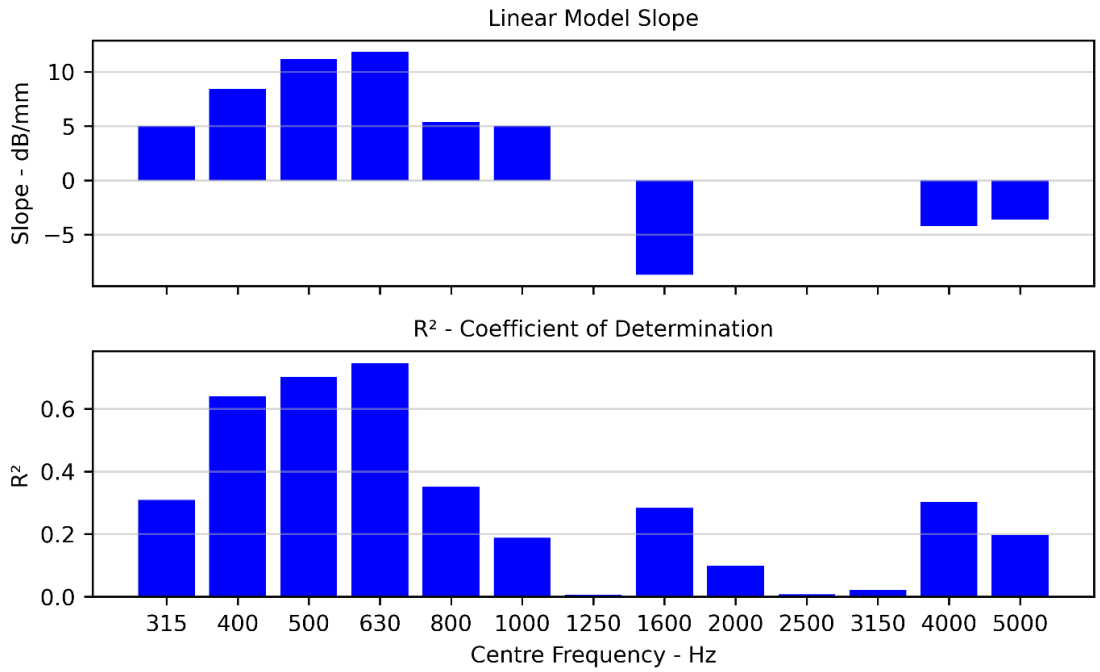


**Figure 23: Correlations and $R^2$ values between one-third octave band levels and MPD for PA7 LV, PA7 HS, PA7, and PA10 on CNC.**

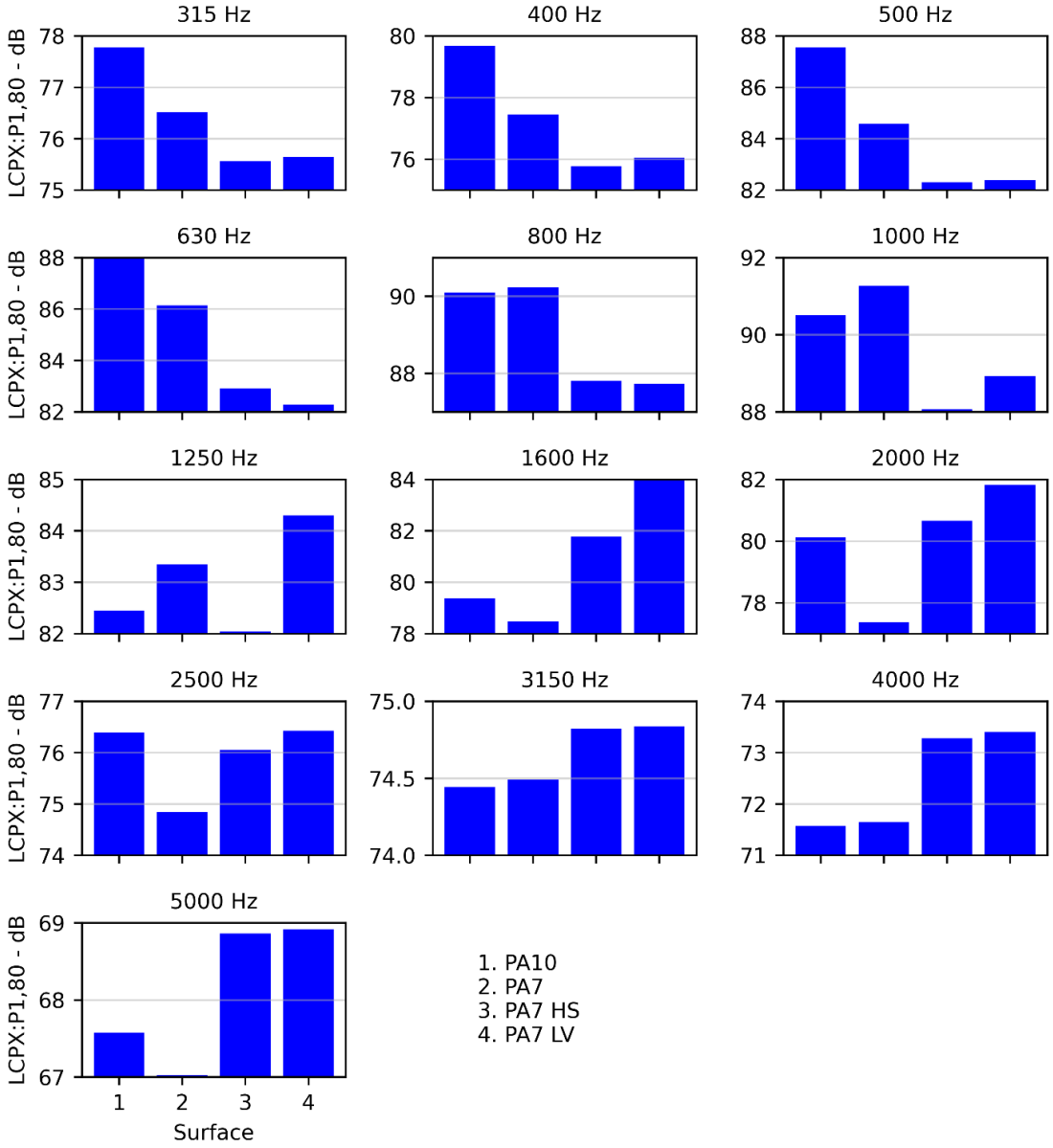


**Figure 24: One-third octave band levels for PA7 LV, PA7 HS, PA7, and PA10 on CNC.**

## Construction Results - Example

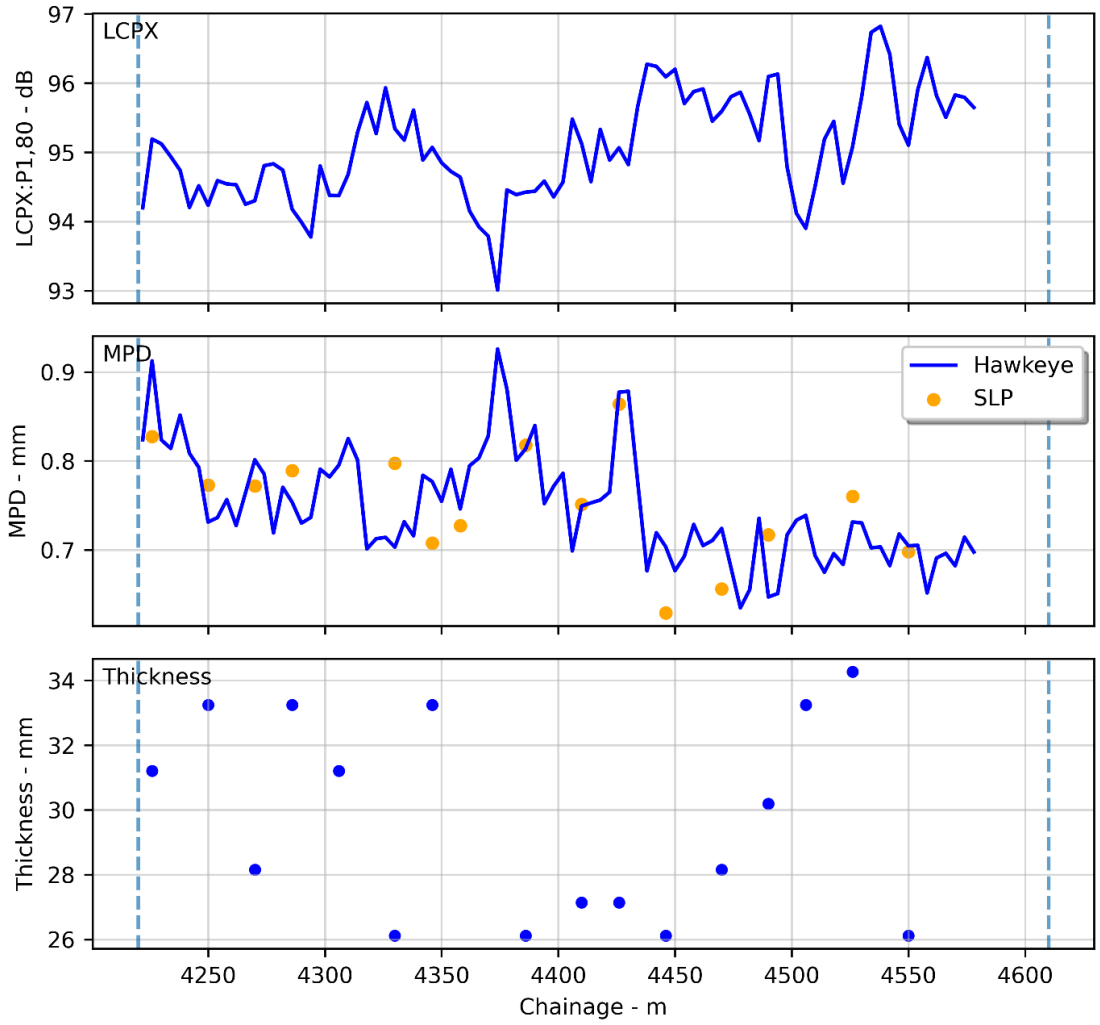


**Figure 25: Longitudinal $L_{CPX}$, MPD (Hawkeye and SLP), and thickness for PA7 LV lane 2 on CNC.**

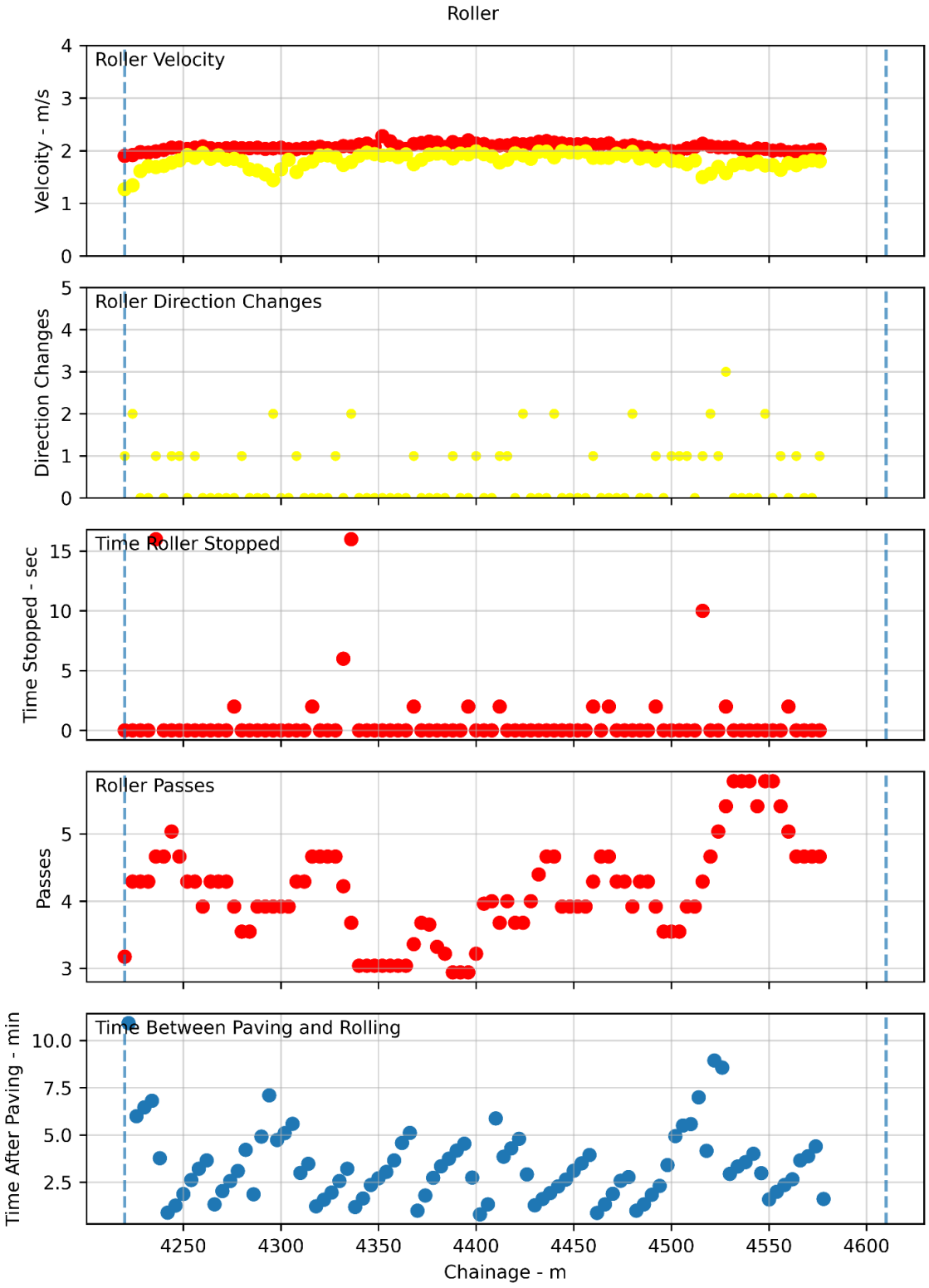


**Figure 26: Longitudinal roller metrics for PA7 LV lane 2 on CNC.**

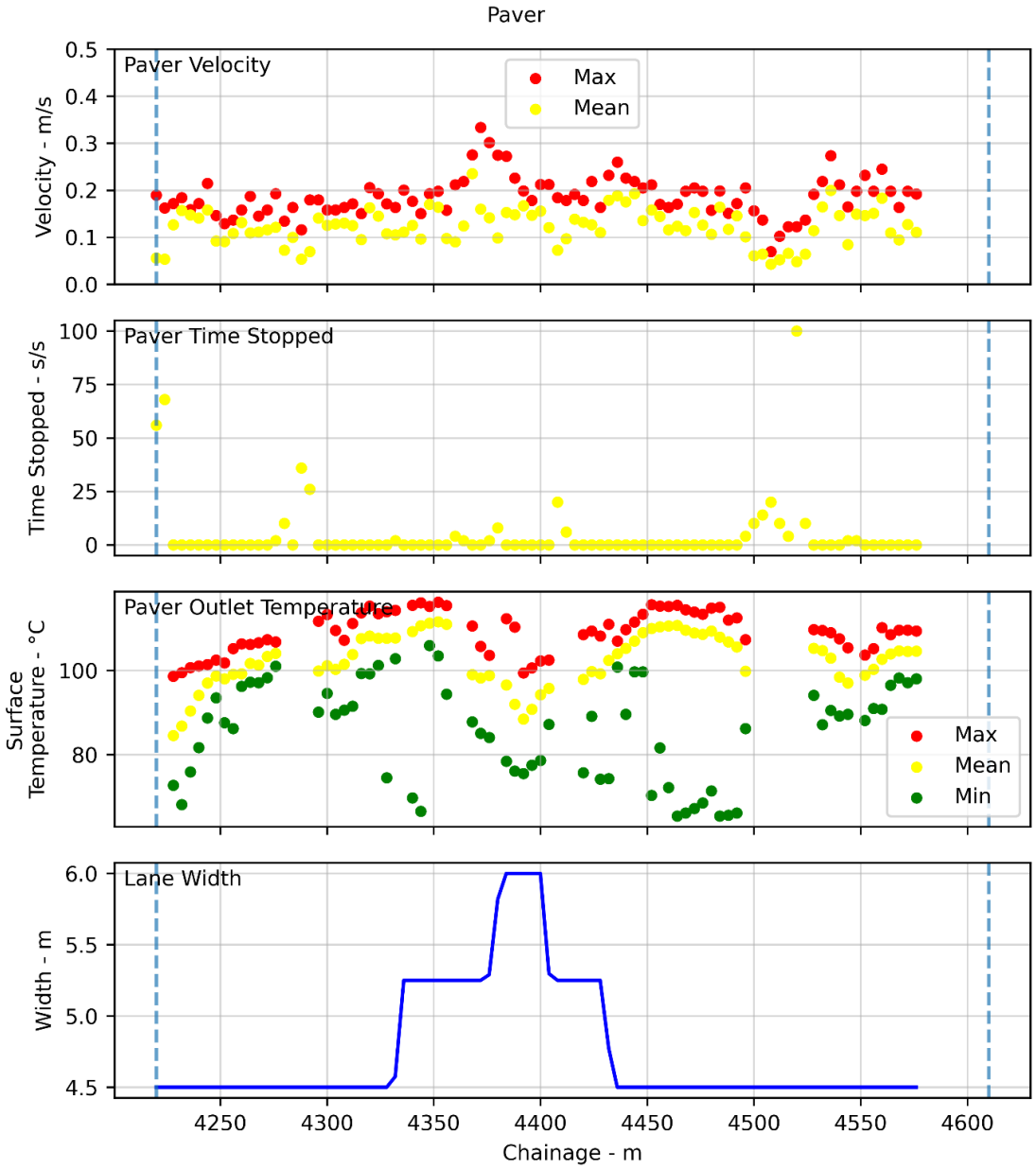


**Figure 27: Longitudinal paving metrics for PA7 LV lane 2 on CNC.**

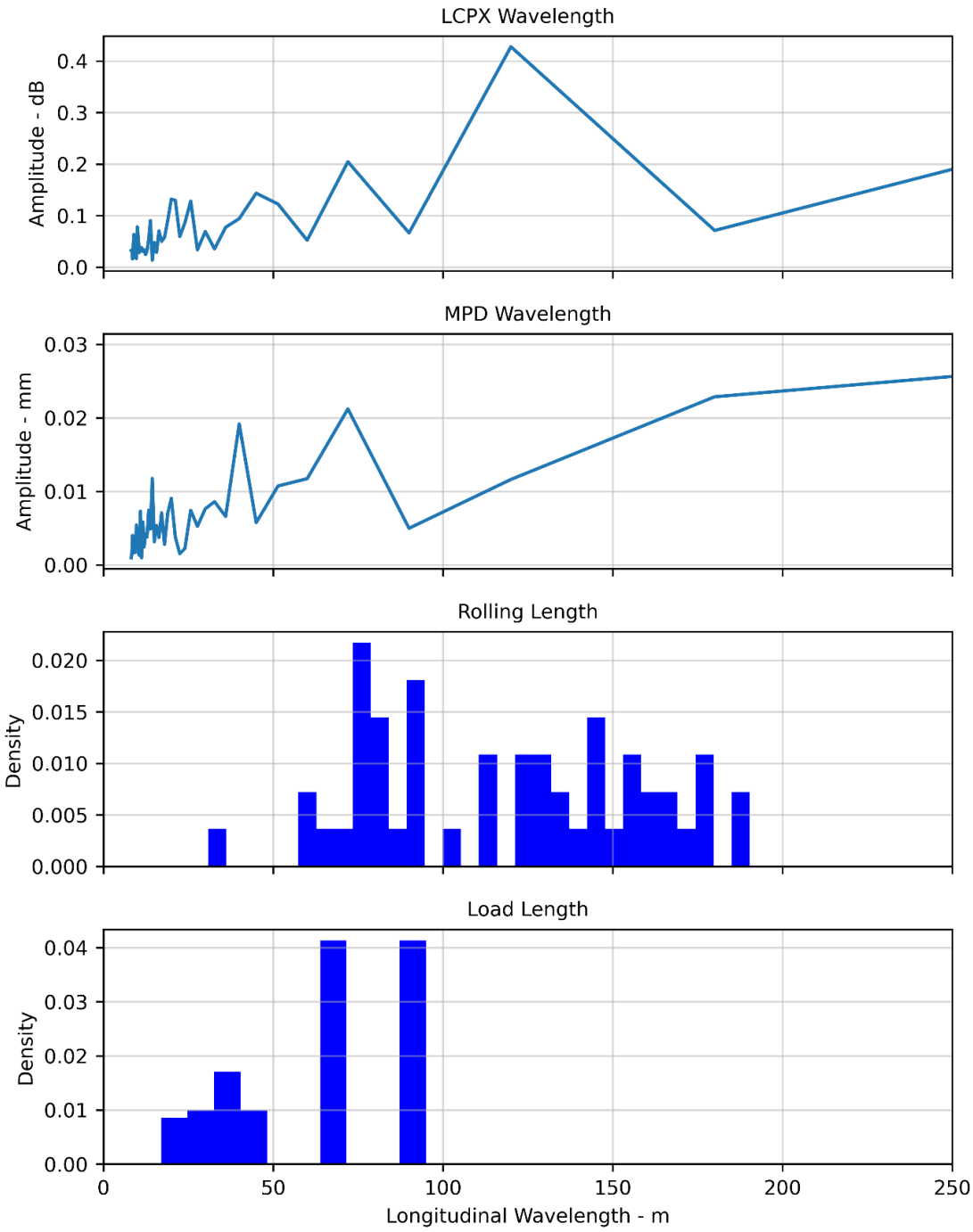


**Figure 28: Longitudinal wavelengths for $L_{CPX}$, MPD, rolling, and asphalt loads for PA7 LV lane 2 on CNC.**

**Table 11: Single variable correlations for PA7 LV lane 2 on CNC.**

| Dependent Variable | Independent Variable | $R^2$ | p-value | Slope |
|---|---|---|---|---|
| mpd_slp | paving_temp_mean | 0.47 | 3.0E-02 | -0.01 |
| right_800 | roller_passes_adj | 0.46 | 1.4E-13 | 1.29 |
| psd_int | paving_temp_max | 0.46 | 3.1E-02 | -0.23 |
| psd_int | paving_temp_mean | 0.44 | 3.7E-02 | -0.17 |
| right_level | roller_passes_adj | 0.43 | 1.9E-12 | 0.95 |
| thickness | paver_v_mean | 0.42 | 6.7E-03 | -54.78 |
| right_1000 | roller_passes_adj | 0.41 | 8.6E-12 | 0.96 |
| right_1600 | roller_passes_adj | 0.41 | 9.0E-12 | 1.62 |
| left_3150 | paving_temp_mean | 0.41 | 3.5E-09 | 0.11 |
| left_4000 | paving_temp_mean | 0.39 | 1.2E-08 | 0.10 |
| indent_depth | roller_v_mean | 0.37 | 1.3E-02 | -0.22 |
| left_2500 | paving_temp_mean | 0.35 | 8.3E-08 | 0.13 |
| right_2000 | roller_passes_adj | 0.35 | 7.9E-10 | 1.53 |
| left_1000 | roller_passes_adj | 0.35 | 9.8E-10 | 0.96 |
| left_2000 | paving_temp_mean | 0.35 | 1.1E-07 | 0.12 |
| left_level | roller_passes_adj | 0.34 | 1.6E-09 | 0.61 |
| right_1250 | roller_passes_adj | 0.33 | 3.3E-09 | 0.79 |
| left_1250 | roller_passes_adj | 0.33 | 3.7E-09 | 1.37 |
| left_1600 | paving_temp_mean | 0.31 | 5.4E-07 | 0.16 |
| left_5000 | paving_temp_mean | 0.31 | 6.2E-07 | 0.10 |
| left_500 | paving_temp_mean | 0.31 | 6.6E-07 | -0.11 |
| left_1250 | paving_temp_mean | 0.27 | 4.4E-06 | 0.15 |
| right_2500 | roller_passes_adj | 0.27 | 2.1E-07 | 1.09 |
| mpd | paving_temp_mean | 0.24 | 1.8E-05 | 0.00 |
| right_4000 | roller_passes_adj | 0.24 | 1.1E-06 | 0.90 |
| left_2000 | roller_v_mean | 0.23 | 1.4E-06 | 4.25 |
| left_1600 | roller_passes_adj | 0.23 | 1.7E-06 | 1.19 |
| left_1000 | paving_temp_mean | 0.22 | 4.7E-05 | 0.09 |
| left_630 | paving_temp_mean | 0.22 | 5.6E-05 | -0.08 |
| left_2000 | time_roller_after_paving | 0.22 | 4.1E-06 | -0.31 |
| right_5000 | roller_passes_adj | 0.21 | 5.6E-06 | 0.88 |

**Table 12: Multi-variable correlations for PA7 LV lane 2 on CNC.**

| Dependent Variable | Independent Variables | | $R^2$ | p-values | |
|---|---|---|---|---|---|
| psd_int | paving_temp_min | paver_v_mean | 0.65 | 0.01 | 0.03 |
| psd_int | paver_v_mean | paving_temp_min | 0.65 | 0.03 | 0.01 |
| left_1250 | paving_temp_mean | roller_passes_adj | 0.57 | 0.00 | 0.00 |
| left_1250 | roller_passes_adj | paving_temp_mean | 0.57 | 0.00 | 0.00 |
| left_1000 | paving_temp_mean | roller_passes_adj | 0.53 | 0.00 | 0.00 |
| left_1000 | roller_passes_adj | paving_temp_mean | 0.53 | 0.00 | 0.00 |
| left_1600 | roller_passes_adj | paving_temp_mean | 0.52 | 0.00 | 0.00 |
| left_1600 | paving_temp_mean | roller_passes_adj | 0.52 | 0.00 | 0.00 |
| left_1600 | roller_passes_adj | roller_v_mean | 0.51 | 0.00 | 0.00 |
| left_1600 | roller_v_mean | roller_passes_adj | 0.51 | 0.00 | 0.00 |
| left_level | roller_passes_adj | paving_temp_max | 0.50 | 0.00 | 0.00 |
| left_level | paving_temp_max | roller_passes_adj | 0.50 | 0.00 | 0.00 |
| left_level | roller_passes_adj | paving_temp_mean | 0.50 | 0.00 | 0.00 |
| left_level | paving_temp_mean | roller_passes_adj | 0.50 | 0.00 | 0.00 |
| left_4000 | paving_temp_max | paving_temp_mean | 0.49 | 0.00 | 0.00 |
| left_4000 | paving_temp_mean | paving_temp_max | 0.49 | 0.00 | 0.00 |
| right_800 | time_roller_after_paving | roller_passes_adj | 0.49 | 0.03 | 0.00 |
| right_800 | roller_passes_adj | time_roller_after_paving | 0.49 | 0.00 | 0.03 |
| right_800 | roller_v_mean | roller_passes_adj | 0.49 | 0.04 | 0.00 |
| right_800 | roller_passes_adj | roller_v_mean | 0.49 | 0.00 | 0.04 |
| left_3150 | paving_temp_mean | paving_temp_max | 0.49 | 0.00 | 0.00 |
| left_3150 | paving_temp_max | paving_temp_mean | 0.49 | 0.00 | 0.00 |

# Appendix B – Project and Trial Section Locations


**Figure 29. Map of CNC, CSM2, and S2G projects.**

# Appendix C – Lane Numbering

(a) Single carriageway

(b) Dual carriageway

**Figure 30. Lane numbering convention.**